The influence of cyclic loading on the response of soft subgrade soil in relation to heavy haul railways

Krishanthan Thevakumar, Ph.D.[1]; Buddhima Indraratna, Ph.D., F.ASCE[2]; Fernanda Bessa Ferreira, Ph.D.[3]; John Carter, M.ASCE[4]; and Cholachat Rujikiatkamjorn, Ph.D., FIEAust[5]

[1]Geotechnical Engineer, GHD, St Leonards NSW 2065, Australia. Formerly, Ph.D. Student, Centre for Geomechanics and Railway Engineering, University of Wollongong, NSW 2522, Australia.
Email: krish.thevakumar@ghd.com

[2]Distinguished Professor of Civil Engineering and Director, Transport Research Centre, University of Technology Sydney, Ultimo NSW 2007, Australia.
Email: buddhima.indraratna@uts.edu.au (Corresponding author)

[3]Postdoctoral Researcher, CONSTRUCT-Geo, Faculty of Engineering, University of Porto, 4200-465 Porto, Portugal. Email: fbf@fe.up.pt

[4]Emeritus Professor, ARC Centre of Excellence for Geotechnical Science and Engineering, University of Newcastle, Callaghan, NSW 2308, Australia. Email: John.Carter@newcastle.edu.au

[5]Professor, School of Civil and Environmental Engineering, University of Technology Sydney, Ultimo NSW 2007, Australia. Email: Cholachat.Rujikiatkamjorn@uts.edu.au

Abstract: The design of rail tracks is often challenged by the highly compressible behaviour of soft estuarine clays over which they must pass. It is prudent that the realistic long-term behaviour of subgrade materials under repeated loading applied by fast moving heavy haul trains is properly understood. One feature that should not be ignored when estimating the long-term performance of track foundations is the continuous principal stress rotation (PSR) induced by moving wheel loads. The main purpose of this research is to combine the traditional cyclic triaxial test results (fixed axes, no PSR) with those obtained from the dynamic hollow cylinder apparatus (allowing PSR) to examine the relative influence of cyclic stress ratio (*CSR*) and frequency on the behaviour of soft subgrade subjected to simulated heavy haul train loading. Employing these two types of equipment applying contrasting stress path regimes, a series of cyclic undrained laboratory tests was conducted on reconstituted sandy clay specimens at varying frequencies (f = 0.1-1 Hz) and cyclic stress ratios (*CSR* = 0.2-0.3). The hollow cylinder test results have shown that higher *CSR* values and lower frequencies induce greater permanent deformations and excess pore water pressures at a given number of loading cycles (N). For *CSR* = 0.2, pore pressures and axial strains were found to increase even after a large number of cycles (N = 50,000). However, when the higher *CSR* value of 0.3 was imposed, the soil failed in less than 300 cycles by reaching 5% of axial strain. Undoubtedly, PSR adversely affected the accumulation of axial strains and soil degradation, whereas in contrast, the development of pore water pressure was less influenced by PSR.

1. Introduction

Over recent years, the rapid growth in population, urbanisation and congestion in highway transport has promoted the adoption of increasingly heavier and faster trains, along with an increase in the frequency of train services. In particular, for railway tracks constructed over soft estuarine subgrade (e.g. silty clays), the long-term repeated train loading produces significant irrecoverable or permanent deformations, and also induces excess pore water pressures in the soil foundation, which adversely affects the design life of the track substructure while exacerbating the cost of maintenance [1-9].

It is well established that the magnitude and orientation of the principal stresses acting on track foundation materials continuously change upon repeated traffic loadings. Fig. 1a illustrates the rotation of the principal stresses acting on a soil element in a track foundation when subjected to moving wheel loads. As the wheel approaches the soil element, the major principal stress (σ_1) increases and reaches its maximum magnitude when the applied load is directly above the soil element. The major principal stress will then decrease once the wheel load moves away from the soil element. The typical stress regime experienced by a soil element in a track foundation is shown in Fig. 1b [10], and the appropriate stress path for this condition was clarified by Gräbe and Clayton [11, 12] using a Finite Element analysis.

In the past, numerous experimental studies have been conducted on fine-grained subgrade soils under cyclic loading conditions to simulate the effects of traffic loading and thereby evaluate the associated deformation behaviour. Although different tests have been performed using dynamic equipment, such as the cyclic triaxial and the resonant column tests, they were often unable to model continuous principal stress rotation (PSR) due to the inability of the test devices. Various studies involving solid cylindrical specimens have been developed over the past few decades to evaluate the effects of cyclic loading in an axisymmetric stress state [13-22]. In all the devices used in these studies, the orientations of the major and minor principal stresses have traditionally been fixed as vertical and horizontal, respectively, except for some loading conditions, such as two-way cyclic loading, in which the direction of principal stresses can be instantaneously changed from 0° to 90° [14, 18]. The true triaxial apparatus enables independent control of the three principal stresses, but it cannot impose the rotation of the principal axes [23-26]. Recent studies conducted using the true triaxial apparatus have examined the three-dimensional stress state of saturated clays under undrained conditions at a constant loading frequency, considering the effects of cyclic intermediate principal stress [24, 25]. Gu et al. [24] introduced a parameter termed as the coefficient of cyclic intermediate principal stress (b_{cyc}) to characterise the coupling effects of cyclic major and intermediate principal stresses, and showed that the permanent major principal strains are inversely proportional to b_{cyc}. Moreover, for the clay used in the aforementioned study, a critical value of $b_{cyc} \approx 0.48$ could be determined, at which the permanent intermediate principal strains transformed from tension to compression. Cyclic load tests on soil specimens under nominal plane strain conditions can be performed using the cyclic simple shear apparatus [27-32]. Although the cyclic simple shear device is capable of rotating the orientation of the principal stresses from -45° to +45° relative to the vertical direction, the changes in the magnitude and orientation of the principal stresses are generally unknown and uncontrollable [33, 34].

To overcome the aforementioned limitations associated with conventional cyclic equipment and more realistically simulate the actual rail traffic-induced stresses in the field, it is necessary to use a versatile equipment, enabling advanced control over both the magnitude and direction of the principal stresses. In the past, the hollow cylinder apparatus has successfully been used to evaluate the effects of PSR in soils, as it allows independent control of up to three principal stresses and the rotation of the principal axes, making more generalised stress path testing possible [11, 12, 35-44]. However, only a few studies have investigated the cyclic stress–strain behaviour of clays under traffic loading using the dynamic hollow cylinder apparatus. In particular, there has been very limited research where laboratory observations from both cyclic hollow cylinder and cyclic triaxial testing under realistic cyclic stress ratios and frequencies have been combined to interpret the soft soil behaviour applicable for railway subgrade. The studies by Gräbe and Clayton [11, 12, 36] involving cyclic hollow cylinder tests have revealed that PSR during cyclic loading has a significant and detrimental effect on the accumulation of permanent deformations and on the resilient modulus of certain types of railroad materials, thus it cannot be ignored when evaluating the actual behaviour of rail tracks. Guo et al. [38] studied the undrained behaviour of a natural clay under traffic loading using a dynamic hollow cylinder apparatus, and they observed that both the cyclic stress magnitude and the loading frequency have a significant influence on the development of vertical strains. Furthermore, compared to the cyclic stress magnitude, the impact of frequency on the resilience behaviour seemed to be secondary. Qian et al. [39] carried out cyclic loading tests using a dynamic hollow cylinder apparatus in addition to cyclic triaxial undrained testing on soft clay, and showed that the accumulated soil deformation responses at different stress levels could be described by the shakedown approach. Cai et al. [41] performed a series of hollow cylinder experiments on soft clay mimicking cardioid-shaped stress paths under different cyclic axial stress and shear stress levels. They observed that when the cyclic stress ratio (*CSR*) was below a threshold value, the shear stress level had little influence on the dynamic behaviour of soft clay. However, with increasing values of *CSR*, the effect of shear stress became more significant, and based on this insightful experimental work, a new model for degradation index was then established.

It is noteworthy that much of the existing cyclic loading research on subgrade soils has been conducted in relation to high-speed rail (i.e. high frequencies and low *CSR*), and that strikingly contrasting conditions prevail for heavy haul rail operations characterised by relatively low speed but much higher axle loads. In the context of heavy haul train loading, the key objective in this study was to combine the traditional cyclic loading triaxial test results (fixed loading axes) with those from dynamic hollow cylinder apparatus (allowing PSR) to examine the relative influence of *CSR* and frequency on the irrecoverable (plastic) soil deformations, build-up of excess pore water pressures and the degradation of soil resilient modulus. In view of the above, the authors have conducted a series of cyclic undrained laboratory tests on reconstituted sandy clay specimens using a dynamic hollow cylinder apparatus (DYNHCA) and a cyclic triaxial apparatus (CTA) employing different frequencies (f = 0.1-1 Hz) and cyclic stress ratios (*CSR* = 0.2-0.3).

Using the Boussinesq theory and the attenuation factors of dynamic stress [2], the stress applied to the point located at a depth of 2.5m from the surface of subgrade corresponds to a *CSR* (defined as the ratio between the deviator stress and twice the effective confining pressure, $CSR = q / 2\, \sigma'_c$) of 0.27 for an axle load of 25 tonnes that is typical of most Australian heavy haul trains. The *CSR* values (0.2 and 0.3) and frequencies (0.1 to 1 Hz) adopted in this study aim to simulate the cyclic loads induced at a depth of 2.5m from the subgrade surface by heavy haul trains travelling at speeds between 40-80 km/h. On a standard gauge track in Australia, while the top of ballast may experience frequencies of up to 20 Hz (i.e. approximately 100 km/h speeds) [45, 46], these attenuate rapidly with depth to the soft subgrade to be of much smaller values, depending on the thickness of subballast and the damping of structural fill over the natural subgrade [47-49]. The selected frequencies in this study (0.1 to 1 Hz) for testing the subgrade soil corroborate mainly with heavy haul trains which only travel at 40-80 km/h in most cases, and very rarely up to 100 km/h.

Although the DYNHCA is capable of applying combined axial-torsional loadings and simulating complex stress paths, some difficulties have been encountered with respect to the test procedures and specimen preparation. In some past studies, hollow cylinder specimens have been prepared from undisturbed block specimens by coring and trimming [37, 50, 51], which may have induced varying levels of disturbance to the mechanical properties of soil. Reconstituted hollow cylinder specimens have been used in this study to ensure the reproducibility and homogeneity of the test specimens. Hence, any influence of the inherent (in situ) soil fabric has been ignored herein.

2. Materials and Methods

2.1. Test Apparatus

The tests reported in this paper were conducted at the University of Wollongong (NSW, Australia), using a dynamic hollow cylinder apparatus, DYNHCA (Fig. 2a) and a cyclic triaxial apparatus, CTA. In the DYNHCA, the external loadings, such as outer cell pressure (P_o), inner cell pressure (P_i), axial load (W) and torque (M_T), can be applied and controlled independently, which allows simulation of a wide range of stress paths for studying the effects of anisotropy, intermediate principal stress ratio and principal stress rotation. Since the axial and torsional loadings are applied simultaneously using frictional end boundary conditions, additional radial stresses are experienced by the soil specimen, which leads to non-linear deformations. Hence, the interpretation of the stress and deformation state within the test specimen requires certain assumptions. In particular, stresses acting along the specimen height and stresses across the wall thickness are assumed to be uniform. The DYNHCA has a configuration for testing under an axial load up to 15kN and a torque up to 400Nm, and it can accommodate hollow cylinder specimens with outer radius (r_e) of 50mm, inner radius (r_i) of 30mm and height (H) of 200mm. By using these specimen dimensions, the stress non-uniformity due to the specimen curvature and the end restraint are reduced to acceptable levels by satisfying the conditions previously recommended by Sayao and Vaid [52] in terms of: (i) wall thickness: $r_e - r_i$ = 20 to 26mm, (ii) inner radius: $0.65 \leq r_i / r_e \leq 0.82$ (a slightly lower value, $r_i / r_e = 0.6$ is obtained with this equipment) and (iii) height: $1.8 \leq H/2r_e \leq 2.2$.

As mentioned, the height of the hollow cylinder specimen is 200mm. The pore water pressures are set to zero at the mid-height of the specimen (i.e. excess pore water pressures are measured at the specimen mid-height). Lateral (radial) pressure is applied by de-aired water against the interior and exterior walls of the test specimen. Digital pressure-volume controllers are connected to the appropriate valves to keep the outer and inner cell pressure as well as the back pressure constant. A dedicated controller applies the back pressure and records the corresponding volume change of the specimen, while the inner and outer cell pressure-volume controllers measure the volume changes inside and outside of the hollow cylinder specimen, respectively. The apparatus has two servo motors, one controlling the axial movement (or load) and the other controlling the torsional movement (or torque). Similar to other types of triaxial apparatus, the axial force and deformation are applied by an actuator at the base of the cell. The torque is applied through the rotation of the same ram imposing the vertical load. The values of axial force and torque are monitored by an internal (submersible) combined load and torque transducer. The axial displacements and rotations are measured through high resolution encoders read by a Digital Control System.

The cyclic triaxial apparatus enables application of a deviatoric cyclic stress while keeping the cell pressure constant throughout the test process. Since it is a conventional device which has been used by several researchers [21, 53], further details about the equipment have been omitted for brevity.

2.2. Specimen Preparation

In this study, reconstituted soil specimens were produced in the laboratory to ensure reproducibility and uniformity. A sandy clay subgrade was simulated by blending kaolin clay with sand in the ratio of 1:1 (based on dry mass), and the basic properties of the kaolin, sand and resulting reconstituted soil are summarised in Table 1.

The hollow cylinder specimens were prepared by using the one-dimensional slurry consolidation method [54-56] according to the following steps:

(1) Sand sieved through the 425μm sieve was mixed with dry kaolin. The soil mixture was thoroughly mixed with de-aired water to obtain a water content of two times the liquid limit [21].

(2) Two custom-made moulds (one mould with inner diameter of 100mm and another with outer diameter of 60mm) were positioned by a 20mm wide annular porous disk at the bottom (Fig. 2b).

(3) The slurry was poured into the cavity between the two moulds which were lubricated with silicone grease at the surfaces (Fig. 2c).

(4) Another 20mm wide annular porous disk was placed on top of the slurry to allow drainage at both ends. The surface of the outer mould was perforated to promote the consolidation process by including radial drainage. The perforated surface was covered with filter paper strips to avoid clogging by soil particles (Fig. 2d).

(5) The specimen was consolidated to a pre-consolidation pressure of 50 kPa in four stages of step loading (i.e., 2 kPa, 7 kPa, 20 kPa and 50 kPa) with approximately 24 hour intervals, when there was no further dissipation of excess pore pressure (Fig. 2e).

(6) Once the consolidation process was completed (after approximately two weeks), according to the ASTM D2435 [57], the hollow cylinder specimen was extruded and trimmed to the desired height. Since an intact hollow cylinder shape was obtained, no coring was required, thereby preventing specimen disturbance. The specimen was then grooved on both top and bottom to fit into the fins of the top and bottom caps of the hollow cylinder chamber (Fig. 2f).

It is noteworthy that clay specimens require different installation procedures from those of sand specimens prior to testing. While sand specimens can be prepared inside the hollow cylinder chamber using dry or moist tamping or pluviation methods, for clay specimens special care needs to be taken while installing the inner and outer rubber membranes, filling inner cell water and fitting fins into the grooved surface of the test specimen after its preparation is completed.

2.3 Saturation and Consolidation

Once the specimen was set up inside the hollow cylinder chamber and filled up with de-aired water, it was saturated by a back pressure of 300 kPa for 72 hours until a Skempton's pore pressure coefficient, $B > 0.96$ was attained. After saturation, the specimen was isotropically consolidated under a mean effective pressure of 50 kPa by applying the same inner and outer cell pressures. This value of stress was chosen to mimic the appropriate confining pressure acting at a depth of around 2.5m from the subgrade surface.

2.4 Test Program

Following isotropic consolidation, a number of cyclic hollow cylinder tests and cyclic triaxial tests were performed under undrained conditions to investigate the effect of frequency, cyclic stress ratio and principal stress rotation on the mechanical behaviour of the test specimens. The undrained conditions herein adopted aim to reproduce the impeded drainage between wheel load cycles under fast moving trains. Loading frequencies ranging from 0.1 to 1 Hz and cyclic stress ratios of 0.2 and 0.3 were employed, whereby all tests were conducted under a constant effective confining pressure of 50 kPa over 50,000 cycles or until failure occurred. Table 2 presents the summary of the testing programme.

The cyclic stress ratio is calculated from the values of the deviator stress (*q*) and effective confining pressure (σ'_c), as:

$$CSR = \frac{q}{2\sigma'_c} \quad (1)$$

where *q* varies cyclically (see later as also represented by Eq. 10).

The resilient modulus (M_R) is a key parameter in the design of railway foundations characterising the foundation soil stiffness with respect to the recoverable strains under repeated loading and unloading imposed by moving traffic. The resilient modulus can thus be determined as:

$$M_R = \frac{q}{\varepsilon_{a,r}} \quad (2)$$

where $\varepsilon_{a,r}$ is the recoverable (resilient) axial strain during unloading [36, 58].

2.5 Stress Status and Stress Paths

The idealised stress state of an element of the hollow cylinder specimen is shown in Fig. 3. Average stresses such as the vertical stress (σ_z), radial stress (σ_r), circumferential stress (σ_θ) and shear stress ($\tau_{z\theta}$) and average strains such as vertical strain (ε_z), radial strain (ε_r), circumferential strain (ε_θ) and shear strain ($\gamma_{z\theta}$) on a soil element were estimated according to Hight et al. [59]. The outer (P_o) and inner (P_i) cell pressures were kept equal to minimise the stress non-uniformity across the wall of the soil specimen, resulting in σ_r and σ_θ being equal to the cell pressure. The ratio of the deviator stress to the shear stress was taken as 2.14 [60].

The major (σ_1) and minor (σ_3) principal stresses were calculated based on the vertical, radial, circumferential and shear stresses, whereas the intermediate principal stress (σ_2) was equal to the radial (σ_r) and circumferential stress (σ_θ). The three principal stresses for the dynamic loading imposed in the hollow cylinder apparatus can be expressed as:

$$\sigma_1 = \frac{(\sigma_z + \sigma_r)}{2} + \sqrt{(\frac{\sigma_z - \sigma_r}{2})^2 + {\tau_{z\theta}}^2} \quad (3)$$

$$\sigma_2 = \sigma_r \quad (4)$$

$$\sigma_3 = \frac{(\sigma_z + \sigma_r)}{2} - \sqrt{(\frac{\sigma_z - \sigma_r}{2})^2 + {\tau_{z\theta}}^2} \quad (5)$$

The magnitude of the intermediate principal stress (σ_2) with respect to the major (σ_1) and minor (σ_3) principal stresses can be characterised by the intermediate principal stress ratio (*b*):

$$b = \frac{\sigma_2 - \sigma_3}{\sigma_1 - \sigma_3} \quad (6)$$

The inclination of the major principal stress direction to the vertical axis (α) can then be calculated from the known stress components as follows:

$$tan\, 2\alpha = \frac{2\, \tau_{z\theta}}{\sigma_z - \sigma_\theta} \quad (7)$$

For the particular case of equal internal and external pressures, the relationship between α and b can be expressed by:

$$b = sin^2\, \alpha \quad (8)$$

In the present study, the intermediate principal stress ratio oscillated from 0 to 0.41 during the loading and unloading process.

To simulate the repetitive train loadings acting on the subgrade, the axial load was first applied to induce a cyclic deviator stress on the specimen. When the maximum deviator stress was reached, a cyclic torsional load was initiated from zero value. A phase difference of 90° between sinusoidal axial and torsional loadings was then established.

When the train wheel load approaches a given soil element, the inclination of the major principal stress reduces from -40° with respect to the vertical direction. The principal stress rotation angle will be zero when the wheel load is directly above the soil element. Then, the orientation of the major principal stress increases to reach a maximum value of +40° as the wheel load moves away from the soil element. The rotation angle will gradually change from +40° to -40° for the next approaching wheel load depending on the spacing between two consecutive wheels. This way, the angle of rotation of the principal stress axis would change between -40° to +40° for every wheel load (Fig. 4a). The value of the rotation angle falls within the range obtained from the study by Gräbe and Clayton [12], which shows that depending on the depth below the track structure, the principal stresses rotate from +/- 90° to +/- 30° before the arrival of the next wheel load. The combination of axial and torsional cyclic loadings produces continuous rotation of the principal stress direction in a circular path, as illustrated in Fig. 4b, which also elaborates how the angle of rotation changes with the shear stress variation. Actual values measured in one representative test (T4) have been compared with predicted (computed) values in Fig. 4 to demonstrate the accuracy of the relatively complex stress path simulated in the hollow cylinder apparatus.

To compare the results from cyclic triaxial apparatus and dynamic hollow cylinder apparatus, the total stress paths should be compared. The mean effective stress (*p'*) and deviator stress (*q*) have been calculated for both types of test using the following equations [61]:

$$p' = \frac{(\sigma'_1 + \sigma'_2 + \sigma'_3)}{3} = \frac{(\sigma'_z + \sigma'_r + \sigma'_\theta)}{3} \quad (9)$$

$$q = \sqrt{\frac{(\sigma_1 - \sigma_2)^2 + (\sigma_1 - \sigma_3)^2 + (\sigma_2 - \sigma_3)^2}{2}} = \sqrt{(\sigma_z - \sigma_\theta)^2 + 3\,\tau_{z\theta}{}^2} \quad (10)$$

As shown in Fig. 5, the total stress paths for cyclic loading with and without PSR follow a similar trend. Therefore, it is reasonable to compare the results obtained from cyclic triaxial tests and hollow cylinder tests.

3. Results and Discussion

It is well known that soil properties are considerably affected by the fabric, stress history and confining pressure [31, 32, 62]. Therefore, these factors were kept constant in this study. A comparison was made between the hollow cylinder test results obtained for different frequencies and cyclic stress ratios in terms of variation of axial deformation, excess pore water pressure and resilient modulus over time (i.e., in relation to the number of cycles). Since all the tests were conducted under undrained conditions, the total volumetric strain (ε_v) was expected to be zero (Eq. 11), and this could be validated by measuring the axial strain (ε_a), radial strain (ε_r) and circumferential strain (ε_θ) of the test specimens, where $\varepsilon_a = -(\varepsilon_r + \varepsilon_\theta)$, based on test T4 (Fig. 6a).

$$\varepsilon_v = \varepsilon_a + \varepsilon_r + \varepsilon_\theta = 0 \quad (11)$$

3.1 Permanent Axial Deformation

Fig. 6b illustrates the axial deformation behaviour of a test specimen during the loading cycles, when a frequency of 1 Hz and a cyclic stress ratio of 0.2 were used (test T4). Also shown here are the measured total, resilient and permanent strains, whereby the increment in the band width of the strain envelope confirms that the resilient strain ($\varepsilon_{a,r}$) increases with the number of cycles (*N*). For clarity and to facilitate the comparison of the axial strains obtained for different test conditions, only the upper and lower limits of the strain envelopes have been plotted in Figs. 7-9.

The effect of frequency on the accumulation of axial strains for cyclic stress ratios of 0.2 and 0.3 is shown in Fig. 7a and b, respectively. As expected, the axial deformations of the test specimens increased with the number of cycles. Regardless of the *CSR* value, the total axial strains were found to decrease with the increasing frequency. For instance, for *CSR* = 0.2 (Fig. 7a), a maximum axial strain of 0.35% was obtained (after *N* = 50,000) under 1 Hz frequency loading, whereas considerably higher strains of 0.48% and 0.58% were reached under lower frequencies (0.5 and 0.1 Hz, respectively). A similar trend was identified in terms of the permanent axial strains (i.e., in general, a low frequency loading induced higher permanent strains when compared to a relatively high frequency loading). It is widely accepted that the loading rate influences the stress-strain behaviour and the yield stress of soil, as the soil yielding is a time-dependent phenomenon. The undrained shear strength of saturated clays increases with the axial strain rate, which can be attributed to lower magnitudes of excess pore water pressures generated during higher strain rates [63-66]. Based on laboratory results from undrained cyclic triaxial testing, Indraratna et al. [67] showed that a lower frequency implies a longer duration for the load to be acting on the soil before unloading within a given cycle, thereby leading to the generation of larger excess pore pressures. As a result, the effective stress decreases and the axial strain increases. Furthermore, for a given imposed stress level, higher strains are developed for slower rates of loading, since adjacent soil particles have time to rearrange themselves in a contractive manner, while creep at inter-particle contacts causes further strain to accumulate [68].

The results presented in Fig. 7a also indicate that for the lower *CSR* value (*CSR* = 0.2), the axial strains increased sharply at the beginning of cyclic loading, with a decreasing increment rate being observed during subsequent cycling. For example, in test T4 (frequency of 1 Hz), the permanent strain reached 0.11% after the first 1000 cycles, whereas an increment of only 0.015% was observed over 10,000 cycles at a later stage (i.e., from cycle 30,000 to cycle 40,000). Moreover, when the highest frequency was applied, the induced permanent deformations nearly stabilised after around 30,000 cycles. However, for the lower frequencies no stabilization occurred during the entire cyclic process. This contrasts with the results from conventional triaxial tests where a steady state is generally reached upon a large number of cycles [16, 21, 53]. As shown in Fig. 7b, for the highest cyclic stress ratio (*CSR* = 0.3), the rate of accumulation of axial deformations tended to increase sharply with the number of cycles, revealing unstable soil behaviour or failure at all frequencies (0.1 to 1 Hz). In fact, in these tests, the specimens failed after a relatively small number of cycles ($N < 300$) by reaching about 5% of axial strain.

Fig. 7c presents the recorded axial strains plotted against time for *CSR* = 0.3 and different loading frequencies. It is observed that the axial deformations produced during a given time interval substantially increase with the loading rate, which can be attributed to the increased number of cycles imposed during that particular period. Indeed, although the magnitude of axial strains decreased with increasing frequency for a given number of loading cycles (Fig. 7b), for the same loading period the higher frequencies lead to more pronounced axial deformations. This is associated with the fact that, for a higher value of *CSR*, the axial deformations increased sharply with increasing number of cycles and therefore, the effect of the number of cycles was predominant concerning the development of axial strains.

To better understand the effect of *CSR* on the accumulation of axial deformations during cyclic loading, Fig. 8 compares the axial strain curves obtained for *CSR* values of 0.2 and 0.3 under the frequency of 0.5 Hz. The plotted results clearly indicate that the *CSR* has a predominant influence on the development of axial strains during the cyclic loading process. For instance, for $N > 100$, the permanent axial strain recorded under *CSR* = 0.3 was about 0.72%, significantly exceeding the value of permanent strain corresponding to *CSR* = 0.2 (0.02%). The total axial strains attained for the same number of cycles increased by tenfold when *CSR* was increased from 0.2 to 0.3. In fact, regardless of the loading rate, the increase in *CSR* led to a substantial increment in both the permanent and total axial strains measured in the tests. This substantial difference in response attributed to an increase in *CSR* from 0.2 to 0.3 indicates that the critical value of *CSR* (i.e. the threshold value beyond which the soil behaves differently, or in an unstable manner) falls between 0.2 and 0.3 for this particular soil when subjected to PSR.

The effect of principal stress rotation on the axial deformation behaviour of soil over the number of cycles for a cyclic stress ratio of 0.2 and different frequencies is presented in Fig. 9a. Regardless of the frequency, the total axial strain at the end of cyclic loading ($N > 50{,}000$) was considerably higher when PSR was imposed (i.e. using the DYNHCA). However, within the first 2,000 cycles, the axial strains induced by cyclic loading without PSR (i.e. using the CTA) exceeded the values obtained from loading with PSR for the frequency of 1 Hz. Regardless of the effect of PSR, the increment rate of axial strain tended to reduce with the number of cycles. While under cyclic loading without PSR, the increment in axial strain was almost negligible after about 40,000 cycles, the axial strain increased continuously with the number of cycles, particularly for the frequency of 0.1 Hz, when PSR was applied. For example, for *CSR* = 0.2 and frequency of 0.1 Hz, the increment in the total axial strain from 40,000 to 50,000 cycles was only 0.012% without PSR, while a higher increment of 0.049% was observed under PSR. Generally, higher axial strain was developed when the cyclic loading was applied with PSR.

For *CSR* of 0.3, the PSR highly affected the development of axial strains, regardless of the frequency (Fig. 9b). At any moment of cyclic loading, the increment of total/plastic axial strain under PSR was significantly higher than that without PSR. For the same *CSR* value (*CSR* = 0.3), soil elements showed a stable behaviour up to 1,000 cycles without PSR, whereas failure was observed within 300 cycles when soil was subjected to PSR. The increment rate of axial strain increased with the loading cycles when the specimen underwent continuous PSR, while without PSR the increment rate tended to reduce throughout the test. For 0.1 Hz frequency loading and after 100 cycles, the total axial strain reached 1% when the load was applied without PSR, whereas an axial strain of 2.5% was obtained in the presence of continuous PSR. Therefore, the threshold value of *CSR* for the soil tested in this study (physical properties specified in Table 1) falls between 0.2 and 0.3 when it is subjected to PSR. However, this critical threshold value of *CSR* exceeds 0.3 when the soil is tested in the triaxial apparatus without any PSR (Fig. 9).

3.2 Excess Pore Water Pressure

Fig. 10a shows the influence of loading rate on the excess pore water pressures generated over the number of cycles for a cyclic stress ratio of 0.2 (i.e., deviator stress of 20 kPa). It can be observed that higher increments of pore water pressure were developed under lower frequencies. Regardless of the frequency, the increment rate of the excess pore water pressures decreased with the number of cycles. For instance, for f = 0.1 Hz, the excess pore water pressure reached 25.8 kPa after the first 10,000 cycles, whereas an increment of only 0.33 kPa was observed over 10,000 cycles at a later stage (i.e., from cycle 30,000 to cycle 40,000). For the highest frequency (1 Hz) the pore water pressures stabilised in less than 20,000 cycles, whereas more than 40,000 cycles were required to reach stabilisation of pore water pressure under a lower frequency of 0.1 Hz.

The evolution of the excess pore water pressures with the number of cycles for a higher *CSR* value (*CSR* = 0.3) is illustrated in Fig. 10b. Similar to what was observed for the lower *CSR* value of 0.2, the pore water pressures recorded during cyclic loading decreased with increasing frequency. Eventually, the soil failed by reaching 5% of axial strain in less than 200 cycles at a frequency of 0.1 Hz, and after about 300 cycles at a significantly higher frequency of 1 Hz. For the same number of cycles, a low frequency loading showed a more detrimental effect on the soft clay response than a higher frequency loading. As previously mentioned, under lower frequencies, the soil fabric has a greater chance to rearrange itself in a contractive manner (i.e. reduced porosity for the same water content), which leads to an increased axial deformation and higher excess pore water pressure. In fact, pore pressure development is time-dependent, and if the frequency is too high, then for the same number of applied loading cycles the loading time of a soil element can be too short to induce significant pore pressure build-up. A similar behaviour has been reported in previous related studies [21, 64, 69]. Consequently, a lower number of cycles would be needed to reach a specified value of excess pore water pressure under a slower rate of loading.

However, if the results are analysed in terms of time rather than the number of cycles (i.e. by plotting the variation of excess pore water pressures with time, as shown in Fig. 10c and d), higher frequency loading generally results in greater excess pore water pressure at a given time. This suggests that at a higher frequency, a larger number of cycles would be required to make the soil unstable, but this could result in an earlier failure, because at a higher frequency more loading cycles are imposed on the soil per unit time. For instance, a train operating at a higher speed could take less time to reach instability, despite needing a larger number of loading cycles.

The effect of the cyclic stress ratio on the evolution of pore water pressures with the number of cycles was also investigated for different frequencies. Fig. 11a compares the variation of excess pore pressures over the number of cycles for *CSR* values of 0.2 and 0.3. As expected, higher stress values lead to higher pore water pressure generation after a given number of cycles, regardless of the frequency. The evolution of excess pore water pressures with time for different *CSR* values as shown in Fig. 11b indicates that higher *CSR* values lead generally to greater excess pore pressure development at a given time. Furthermore, for the test conditions considered herein (i.e. relatively high values of *CSR* corroborating with heavy haul trains), the variation of *CSR* was found to have a greater influence on the development of pore water pressures than the variation of frequency (Fig. 11). For instance, for *N* = 200 cycles, and if a constant *CSR* value of 0.3 is considered, the increment of pore water pressure attributed to the variation of frequency from 1 to 0.1 Hz was 9.2 kPa, whereas a larger increment of pore water pressure of 21.1 kPa was observed upon the variation of *CSR* from 0.2 to 0.3, considering a constant frequency of 0.1 Hz and for *N* = 200 cycles (Fig. 11a). In this study, the accumulation of excess pore water pressures upon cyclic loading increased up to 193% with increasing *CSR* (from 0.2 to 0.3) and up to 40% with the decreasing frequency (from 1 to 0.1 Hz). These results clearly imply that when considering heavy haul loading conditions, the development of excess pore water pressures is primarily a function of the applied *CSR* (axle loads) and of secondary influence of frequency (speed) at high *CSR* values. At high *CSR* values corroborating with heavy haul trains with axle loads of up to 35 tonnes (common in Australia), their much slower speeds often less than 70 km/h allow this high axle loading to be applied over a longer period of time for the same number of cycles. Therefore, under prevailing undrained conditions, the build-up of pore water pressures can be greater than for situations corresponding to higher frequencies applied over a much shorter period of time.

Fig. 12 illustrates the influence of continuous rotation of principal stress direction on the accumulation of excess pore water pressure for *CSR* of 0.2 (Fig. 12a) and 0.3 (Fig. 12b). It can be observed that the excess pore water pressure increased with the number of cycles at a progressively decreasing rate, regardless of the frequency and PSR. For *CSR* = 0.2, the presence of PSR (i.e. in the DYNHCA tests) had no significant effect on the increment of pore water pressure with the number of cycles. Even though the values of excess pore water pressure achieved after 50,000 cycles were similar both with and without PSR, the stabilisation of pore pressure occurred at a lower number of cycles when no PSR was applied. For example, for *f* = 0.1 Hz loading from cycle 10,000 to cycle 20,000, the increment of the excess pore water pressure was 2.15 kPa when the specimen was subjected to continuous PSR, whereas the increment was only 0.04 kPa when the soil was not subjected to PSR (Fig. 12a).

Fig. 12b compares the evolution of excess pore water pressure as function of the number of cycles with and without PSR (i.e. during DYNHCA and CTA tests, respectively) for a *CSR* value of 0.3. Under a relatively low frequency of 0.1 Hz, the effect of PSR on the development of excess pore water pressure can be considered negligible. However, at a higher frequency of 1 Hz, a visible increment in pore pressure was observed when PSR was applied. For instance, after 200 cycles, the increments in excess pore water pressure were 0.2 kPa and 10 kPa for the frequencies of 0.1 and 1 Hz, respectively. For a frequency of 0.1 Hz, the soil specimen under PSR failed in 200 cycles by reaching an excess pore pressure of 32 kPa, whereas without PSR the soil showed a stable behaviour up to 1,000 cycles and the excess pore water pressure increased up to 40 kPa. This is because the soil specimen failed by reaching an axial strain of 5% after 200 cycles, when the specimen was subjected to continuous rotation of principal stress direction.

3.3. Resilient Modulus

The hysteretic (stress-strain) loops allow investigating the degradation behaviour of the soil specimen under cyclic loading. This can be characterised by the variation of the resilient modulus. In the current study, the resilient modulus (M_R) was computed according to Eq. (2) at specific numbers of cycles, and subsequently normalised with respect to the value obtained in the first cycle (N = 1). This ratio can be designated as the degradation index (δ), as proposed by Idriss et al [27]:

$$\delta = \frac{(M_R)_N}{(M_R)_1} = \frac{\frac{q}{(\varepsilon_{a,r})_N}}{\frac{q}{(\varepsilon_{a,r})_1}} = \frac{(\varepsilon_{a,r})_1}{(\varepsilon_{a,r})_N} \qquad (12)$$

To evaluate the effect of frequency on the resilient strain of the test specimens, the variation of the normalised M_R with the number of cycles (degradation curve) was plotted in Fig. 13a for the *CSR* value of 0.2. Fig. 13b illustrates the influence of *CSR* on the degradation of M_R during cyclic loading. Regardless of the frequency and *CSR* values, the test results could be fitted well to a logarithm trend line with $R^2 > 0.95$, as given by:

$$\delta = a \ln(N) + 1 \qquad (13)$$

where, a is an empirical constant depending on frequency.

According to the results presented in Fig. 13, a relatively fast degradation of M_R occurred in the first few cycles with a more gradual decreasing trend being observed during subsequent cycling. In particular, for *CSR* = 0.2 (Fig. 13a) and frequency of 1 Hz, the normalised M_R decreased from 1 to 0.68 in the first 1,000 cycles while a slight reduction of 0.03 was observed between 40,000 and 50,000 cycles, which implies that the slope of the hysteretic loop was reduced at a higher rate within the first 1,000 cycles, and the rate of reduction in slope was diminished in the subsequent cycles [32, 61]. Additionally, the reduction in the magnitude of M_R was more pronounced at lower frequencies, regardless of the *CSR* value. For example, for *CSR* = 0.2, the slope of the logarithm line (a) was determined as -0.087 for 0.1 Hz, whereas the value of -0.056 was obtained for 1 Hz. As expected, the higher the *CSR* value, the greater would be the degradation of M_R with increasing *N* (Fig. 13b).

Fig. 14a compares the values of the normalised M_R measured in the tests conducted with and without PSR (i.e. using the DYNHCA and the CTA, respectively) for a *CSR* of 0.2 and different frequencies. Regardless of PSR, the normalised M_R decreased sharply at the early stage of cyclic loading and the reduction rate declined during subsequent cycling. Regardless of the frequency, the influence of PSR on the degradation of M_R was substantial with the soil specimen showing more pronounced degradation behaviour when subjected to PSR (i.e. during DYNHCA tests). The effect of PSR on δ for *CSR* of 0.3 is shown in Fig. 14b, which clearly indicates that the inclusion of continuous PSR led to a quicker degradation, and the soil failure occurred in a few cycles. In particular, for 0.1 Hz frequency, the application of the first 100 loading cycles without PSR degraded the normalised M_R of soil from 1 to 0.79, whereas the normalised M_R decreased to 0.19 under the same number of cycles when continuous PSR was imposed. Fig. 14b also shows that lower frequency loading induced greater degradation compared to the higher frequency loading both with and without PSR. In a heavy haul loading perspective, these results infer that the soil deformation in relation to the resilient modulus will be significantly underestimated if the effect of *PSR* is not considered [61].

The values of the initial M_R (i.e., M_R measured in the first load cycle) obtained from the cyclic hollow cylinder tests for different test conditions are presented in Fig. 15. It can be observed that the initial M_R increases with the loading frequency at a progressively decreasing rate. Higher values of initial M_R were obtained for the *CSR* of 0.2, in comparison to those for *CSR* of 0.3. In fact, when a *CSR* of 0.3 was imposed, the resilient axial strains measured in the first load cycle were significantly greater than those for *CSR* of 0.2. As a result, the values of the initial M_R for *CSR* = 0.3 were about 23-31% lower than those for *CSR* = 0.2, depending on the loading frequency. Therefore, the selection of the appropriate resilient modulus for a specific soft subgrade depending on the applied stress level (axle load) and the train speed is vital in practice.

4. Conclusions

A series of tests was conducted using a dynamic hollow cylinder apparatus (DYNHCA) and a cyclic triaxial apparatus to investigate the mechanical response of soft soil under continuous cyclic loading. Reconstituted (sandy clay) hollow cylinder specimens were produced using a slurry consolidation method. The effect of frequency, cyclic stress ratio (*CSR*) and principal stress rotation (PSR) on the evolution of permanent deformations, excess pore water pressures and degradation of resilient modulus (M_R) was evaluated and discussed. Based on the obtained results, the following conclusions can be drawn.

- Complex stress paths involving PSR can be simulated using the DYNHCA with 90° phase difference between sinusoidal axial and torsional loadings. The intended stress paths were successfully controlled in the apparatus.
- Both resilient (recoverable) and plastic axial strains are induced by cyclic PSR. As expected, the axial deformations of the test specimens increased with the number of cycles. Higher stress values (*CSR* = 0.3) and lower frequencies (0.1 and 0.5 Hz) led to increased permanent deformations. For the test conditions analysed, the influence of the *CSR* on the accumulation of permanent strains was found to be more significant than that of frequency.

- The accumulation of excess pore water pressures upon cyclic loading increased with the *CSR* (up to 193%) and with the decreasing frequency (up to 40%).
- The slope of the stress-strain hysteretic loops decreased with the number of cycles (*N*), representing the degradation of M_R. The reduction in M_R was more pronounced under lower frequencies (0.1 and 0.5 Hz) and higher *CSR* (*CSR* = 0.3). For *CSR* = 0.2, the degradation increased progressively and no steady state was reached after about *N* = 50,000.
- The value of M_R recorded in the first load cycle of the hollow cylinder tests increased with the loading rate (up to 28%) and with the decreasing *CSR* (up to 46%).
- The influence of PSR on the development of axial strains under cyclic loading was relevant and became more pronounced with increasing *CSR*. However, in general, PSR did not significantly affect the pore water pressure increment, particularly when the lower *CSR* value was applied (*CSR* = 0.2).
- Regardless of frequency and *CSR*, the degradation of M_R increased substantially by the presence of PSR.

The results reported herein provide important insight into the long-term performance of low-plasticity soft soil (reconstituted sandy clay) subjected to moving wheel loads, considering the role of PSR. Future studies involving additional parameters, such as soil plasticity, anisotropy and stress level would be useful to provide further insight following the above conclusions. Since the degradation of M_R may have a predominant influence on the design life of railway foundations (natural subgrade), practitioners should consider the variations of M_R evaluated under realistic loading (incorporating PSR) for improved track design and performance evaluation.

CRediT authorship contribution statement

Krishanthan Thevakumar: Formal analysis, Investigation, Methodology, Writing - original draft. Buddhima Indraratna: Conceptualization, Investigation, Methodology, Supervision, Writing - review & editing. Fernanda Bessa Ferreira: Formal analysis, Investigation, Supervision, Writing - review &

editing. John Carter: Supervision, Writing - review & editing. Cholachat Rujikiatkamjorn: Supervision, Writing - review & editing.

Acknowledgements

This research was funded by the Australian Research Council (ARC) through the ARC Linkage scheme. The laboratory assistance from technical officers Alan Grant and Richard Berndt in the School of Civil, Mining and Environmental Engineering at the University of Wollongong is gratefully appreciated. The third author is also grateful for the financial support by: Project PTDC/ECI-EGC/30452/2017-POCI-01-0145-FEDER-030452 - funded by FEDER funds through COMPETE2020 - Programa Operacional Competitividade e Internacionalização (POCI) and by national funds (PIDDAC) through FCT/MCTES, and Programmatic funding - UIDP/04708/2020 of the CONSTRUCT - Instituto de I&D em Estruturas e Construções - funded by national funds through the FCT/MCTES (PIDDAC).

References

[1] Arulrajah A, Abdullah A, Bo MW, Bouazza A. *Ground improvement techniques for railway embankments.* Proceedings of the Institution of Civil Engineers: Ground Improvement 2009; **162**(1):3-14.

[2] Liu J, Xiao J. *Experimental study on the stability of railroad silt subgrade with increasing train speed.* Journal of Geotechnical and Geoenvironmental Engineering 2009; **136**(6):833-841.

[3] Arulrajah A, Abdullah A, Bo MW, Leong M. *Geosynthetic applications in high-speed railways: A case study.* Proceedings of the Institution of Civil Engineers: Ground Improvement 2015; **168**(1):3-13.

[4] Indraratna B, Ferreira FB, Qi Y, Ngo TN. *Application of geoinclusions for sustainable rail infrastructure under increased axle loads and higher speeds.* Innovative Infrastructure Solutions 2018; **3**(1):69.

[5] Dong K, Connolly DP, Laghrouche O, Woodward PK, Alves Costa P. *The stiffening of soft soils on railway lines.* Transportation Geotechnics 2018; **17**:178-191.

[6] Ngo TN, Indraratna B, Rujikiatkamjorn C. *Improved performance of ballasted tracks under impact loading by recycled rubber mats.* Transportation Geotechnics 2019; **20**:100239.

[7] Zhou S, Wang B, Shan Y. *Review of research on high-speed railway subgrade settlement in soft soil area.* Railway Engineering Science 2020; **28**(2):129-145.

[8] Indraratna B, Ngo T, Ferreira F, Rujikiatkamjorn C, Shahkolahi A. *Laboratory examination of ballast deformation and degradation under impact loads with synthetic inclusions.* Transportation Geotechnics 2020; **25**:100406.

[9] Indraratna B, Ngo T, Ferreira F, Rujikiatkamjorn C, Tucho A. *Large-scale testing facility for heavy haul track.* Transportation Geotechnics 2021; **28**:100517.

[10] Brown SF. *Soil mechanics in pavement engineering.* Geotechnique 1996; **46**(3):383-426.

[11] Gräbe PJ, Clayton CR. *Effects of principal stress rotation on permanent deformation in rail track foundations.* Journal of Geotechnical and Geoenvironmental Engineering 2009; **135**(4):555-565.

[12] Gräbe PJ, Clayton CR. *Permanent deformation of railway foundations under heavy axle loading*. In *International Heavy Haul Conference*. 2003. International Heavy Haul Association, Dallas, Texas, USA. p. 325-333.

[13] Sangrey DA, Henkel DJ, Esrig MI. *The effective stress response of a saturated clay soil to repeated loading.* Canadian Geotechnical Journal 1969; **6**(3):241-252.

[14] Brown SF, Lashine AK, Hyde AF. *Repeated load triaxial testing of a silty clay.* Geotechnique 1975; **25**(1):95-114.

[15] Lee KL, Focht JA. *Strength of clay subjected to cyclic loading.* Marine Geotechnology 1976; **1**(3):165-185.

[16] Yasuhara K, Yamanouchi T, Hirao K. *Cyclic strength and deformation of normally consolidated clay.* Soils and Foundations 1982; **22**(3):77-91.

[17] Hyde AF, Ward SJ. *The effect of cyclic loading on the undrained shear strength of a silty clay.* Marine Geotechnology 1986; **6**(3):299-314.

[18] Andersen KH. *Properties of soft clay under static and cyclic loading.* Norwegian Geotechnical Institute 1988; **176**:1-20.

[19] Hyde AF, Yasuhara K, Hirao K. *Stability criteria for marine clay under one-way cyclic loading.* Journal of Geotechnical Engineering 1993; **119**(11):1771-1789.

[20] Jiang M, Cai Z, Cao P, Liu D. *Effect of cyclic loading frequency on dynamic properties of marine clay*. In *GeoShanghai International Conference - Soil Dynamics and Earthquake Engineering*. 2010. Shanghai, China. p. 240-245.

[21] Ni J, Indraratna B, Geng X, Rujikiatkamjorn C. *The effect of the strain rate on soft soil behaviour under cyclic loading*. In *11th Australia-New Zealand Conference on Geomechanics*. 2012. Australia: Engineers Australia. p. 1340-1345.

[22] Xu Z, Pan L, Gu C, Wang J, Cai Y. *Deformation behavior of anisotropically overconsolidated clay under one-way cyclic loading.* Soil Dynamics and Earthquake Engineering 2020; **129**:105943.

[23] Wood DM. *Explorations of principal stress space with kaolin in a true triaxial apparatus.* Geotechnique 1975; **25**(4):783-797.

[24] Gu C, Gu Z, Cai Y, Wang J, Dong Q. *Effects of cyclic intermediate principal stress on the deformation of saturated clay.* Journal of Geotechnical and Geoenvironmental Engineering 2018; **144**(8):04018052.

[25] Gu C, Wang Y, Cui Y, Cai Y, Wang J. *One-way cyclic behavior of saturated clay in 3D stress state.* Journal of Geotechnical and Geoenvironmental Engineering 2019; **145**(10):04019077.

[26] Pang Y, Gu C, Wang J, Cai Y. *Strain evolution of saturated clays under cyclic loadings in three-dimensional stress condition.* Engineering Geology 2020; **278**:105824.

[27] Idriss IM, Dobry R, Sing R. *Nonlinear behavior of soft clays during cyclic loading.* Journal of Geotechnical and Geoenvironmental Engineering 1978; **104**(12):1427-1447.

[28] Seed HB, Idriss IM, *On the importance of dissipation effects in evaluating pore pressure changes due to cyclic loading*, in *Soil mechanics - Transient and cyclic loads. Constitutive relations and numerical treatment*. 1982, Wiley, Chichester, UK.

[29] Vucetic M. *Normalized behavior of offshore clay under uniform cyclic loading.* Canadian Geotechnical Journal 1988; **25**(1):33-41.

[30] Kagawa T. *Moduli and damping factors of soft marine clays.* Journal of Geotechnical Engineering 1992; **118**(9):1360-1375.

[31] Lefebvre G, Pfendler P. *Strain rate and preshear effects in cyclic resistance of soft clay.* Journal of Geotechnical Engineering 1996; **122**(1):21-26.

[32] Mortezaie AR, Vucetic M. *Effect of frequency and vertical stress on cyclic degradation and pore water pressure in clay in the NGI simple shear device.* Journal of Geotechnical and Geoenvironmental Engineering 2013; **139**(10):1727-1737.

[33] Arthur JR, Menzies BK. *Inherent anisotropy in a sand.* Geotechnique 1972; **22**(1):115-128.

[34] Arthur JR, Chua KS, Dunstan T. *Dense sand weakened by continuous principal stress direction rotation.* Geotechnique 1979; **29**(1):91-96.

[35] Shen Y, Zhou J, Gong XN, Liu HL. *Intact soft clay's critical response to dynamic stress paths on different combinations of principal stress orientation.* Journal of Central South University of Technology (English Edition) 2008; **15**(SUPPL. 2):147-154.

[36] Gräbe PJ, Clayton CR. *Effects of principal stress rotation on resilient behavior in rail track foundations.* Journal of Geotechnical and Geoenvironmental Engineering 2014; **140**(2):04013010.

[37] Zhou J, Xu C. *Impact of shear stress on strain and pore water pressure behavior of intact soft clay under principal stress rotation.* Geotechnical Testing Journal 2014; **37**(3):447-462.

[38] Guo L, Chen J, Wang J, Cai Y, Deng P. *Influences of stress magnitude and loading frequency on cyclic behavior of K0-consolidated marine clay involving principal stress rotation.* Soil Dynamics and Earthquake Engineering 2016; **84**:94-107.

[39] Qian JG, Wang YG, Yin ZY, Huang MS. *Experimental identification of plastic shakedown behavior of saturated clay subjected to traffic loading with principal stress rotation.* Engineering Geology 2016; **214**:29-42.

[40] Wang Y, Gao Y, Li B, Fang H, Wang F, Guo L, Zhang F. *One-way cyclic deformation behavior of natural soft clay under continuous principal stress rotation.* Soils and Foundations 2017; **57**(6):1002-1013.

[41] Cai Y, Wu T, Guo L, Wang J. *Stiffness degradation and plastic strain accumulation of clay under cyclic load with principal stress rotation and deviatoric stress variation.* Journal of Geotechnical and Geoenvironmental Engineering 2018; **144**(5):04018021.

[42] Wang Y, Gao Y, Cai Y, Guo L. *Effect of initial state and intermediate principal stress on noncoaxiality of soft clay-involved cyclic principal stress rotation.* International Journal of Geomechanics 2018; **18**(7):04018081.

[43] Wang Y, Gao Y, Li B, Guo L, Cai Y, Mahfouz AH. *Influence of initial state and intermediate principal stress on undrained behavior of soft clay during pure principal stress rotation.* Acta Geotechnica 2019; **14**(5):1379-1401.

[44] Yang Q, Tang Y, Yuan B, Zhou J. *Cyclic stress–strain behaviour of soft clay under traffic loading through hollow cylinder apparatus: effect of loading frequency.* Road Materials and Pavement Design 2019; **20**(5):1026-1058.

[45] Indraratna B, Nimbalkar S, Rujikiatkamjorn C. *From theory to practice in track geomechanics – Australian perspective for synthetic inclusions.* Transportation Geotechnics 2014; **1**(4):171-187.

[46] Sun QD, Indraratna B, Nimbalkar S. *Deformation and degradation mechanisms of railway ballast under high frequency cyclic loading.* Journal of Geotechnical and Geoenvironmental Engineering 2016; **142**(1):04015056.

[47] Powrie W, Yang LA, Clayton CRI. *Stress changes in the ground below ballasted railway track during train passage.* Proceedings of the Institution of Mechanical Engineers, Part F: Journal of Rail and Rapid Transit 2007; **221**(2):247-261.

[48] Liu J, Xiao J. *Experimental study on the stability of railroad silt subgrade with increasing train speed.* Journal of Geotechnical and Geoenvironmental Engineering 2010; **136**(6):833-841.

[49] Ni J, Indraratna B, Geng XY, Carter JP, Rujikiatkamjorn C. *Radial consolidation of soft soil under cyclic loads.* Computers and Geotechnics 2013; **50**:1-5.

[50] Yan JJ, Zhou J, Gong XN, Cao Y. *Undrained response of reconstituted clay to cyclic pure principal stress rotation.* Journal of Central South University 2015; **22**(1):280-289.

[51] Wang J, Feng D, Guo L, Fu H, Cai Y, Wu T, Shi L. *Anisotropic and noncoaxial behavior of K0-consolidated soft clays under stress paths with principal stress rotation.* Journal of Geotechnical and Geoenvironmental Engineering 2019; **145**(9):04019036.

[52] Sayao A, Vaid YP. *Critical assessment of stress nonuniformities in hollow cylinder test specimens.* Soils and Foundations 1991; **31**(1):60-72.

[53] Guo L, Wang J, Cai Y, Liu H, Gao Y, Sun H. *Undrained deformation behavior of saturated soft clay under long-term cyclic loading.* Soil Dynamics and Earthquake Engineering 2013; **50**:28-37.

[54] Lin H, Penumadu D. *Experimental investigation on principal stress rotation in Kaolin clay.* Journal of Geotechnical and Geoenvironmental Engineering 2005; **131**(5):633-642.

[55] Sheeran DE, Krizek RJ. *Preparation of homogeneous soil samples by slurry consolidation.* J Mater 1971; **6**(2):356-373.

[56] Tastan EO, Carraro JA. *A new slurry-based method of preparation of hollow cylinder specimens of clean and silty sands.* Geotechnical Testing Journal 2013; **36**(6):811-822.

[57] ASTM D2435. Standard test method for one-dimensional consolidation properties of soils. ASTM, West Conshohocken, PA; 1996.

[58] Indraratna B, Vinod JS, Lackenby J. *Influence of particle breakage on the resilient modulus of railway ballast.* Géotechnique 2009; **59**(7):643-646.

[59] Hight DW, Gens A, Symes MJ. *The development of a new hollow cylinder apparatus for investigating the effects of principal stress rotation in soils.* Geotechnique 1983; **33**(4):355-383.

[60] Gräbe PJ, *Resilient and permanent deformation of railway foundations under principal stress rotation*. 2002, PhD Thesis, University of Southampton, UK.

[61] Qian J, Du Z, Lu X, Gu X, Huang M. *Effects of principal stress rotation on stress–strain behaviors of saturated clay under traffic–load–induced stress path.* Soils and Foundations 2019; **59**(1):41-55.

[62] Vucetic M, Dobry R. *Effect of soil plasticity on cyclic response.* Journal of Geotechnical Engineering 1991; **117**(1):89-107.

[63] Richardson AM, Whitman RV. *Effect of strain-rate upon undrained shear resistance of a saturated remoulded fat clay.* Geotechnique 1963; **13**(4):310-324.

[64] Lefebvre G, Leboeuf D. *Rate effects and cyclic loading of sensitive clays.* Journal of Geotechnical Engineering 1987; **113**(5):476-489.

[65] Mun W, Teixeira T, Balci MC, Svoboda J, McCartney JS. *Rate effects on the undrained shear strength of compacted clay.* Soils and Foundations 2016; **56**(4):719-731.

[66] Yang C, Carter JP, Sheng D, Sloan SW. *An isotach elastoplastic constitutive model for natural soft clays.* Computers and Geotechnics 2016; **77**:134-155.

[67] Indraratna B, Singh M, Nguyen TT, Leroueil S, Abeywickrama A, Kelly R, Neville T. *Laboratory study on subgrade fluidization under undrained cyclic triaxial loading.* Canadian Geotechnical Journal 2020; **57**(11):1767-1779.

[68] Terzaghi K, Peck RB, Mesri G, *Soil mechanics in engineering practice*. 1996: John Wiley & Sons.

[69] Jiang Y, Lei HY, Zheng G, Yang XJ. *Fractal study of microstructure variation of structured clays under dynamic loading.* Yantu Lixue/Rock and Soil Mechanics 2010; **31**(10):3075-3080.

Figure Captions

Fig. 1. (a) Principal stress rotation in soil under moving wheel loads; (b) stress conditions under a single moving wheel load (after Brown 1996)

Fig. 2. (a) Schematic diagram of the hollow cylinder apparatus; (b) moulds positioned by the bottom porous disk; (c) pouring slurry; (d) top porous disk positioned over slurry; (e) consolidation; (f) grooved soil specimen

Fig. 3. Stress status in a hollow cylinder specimen: (a) external loadings; (b) local stresses on an element; (c) principal stresses on an element

Fig. 4. Effect of moving wheel loads on: (a) rotation angle; (b) shear stresses

Fig. 5. Comparison of total stress path for cyclic loading with and without PSR

Fig. 6. (a) Variation of mean values of axial, radial and circumferential strain with the number of cycles (test T4); (b) variation of axial strain with the number of cycles showing the different strain components (test T4)

Fig. 7. Effect of frequency on the accumulation of axial deformations: (a) *CSR* = 0.2; (b) *CSR* = 0.3 (strains plotted against the number of cycles); (c) *CSR* = 0.3 (strains plotted against time)

Fig. 8. Effect of *CSR* on the accumulation of axial deformations (*f* = 0.5 Hz)

Fig. 9. Effect of PSR on the accumulation of axial deformations: (a) *CSR* = 0.2; (b) *CSR* = 0.3

Fig. 10. Effect of frequency on the development of excess pore water pressures: (a) *CSR* = 0.2 (plotted against the number of cycles; (b) *CSR* = 0.3 (plotted against the number of cycles); (c) *CSR* = 0.2 (plotted against time); (d) *CSR* = 0.3 (plotted against time)

Fig. 11. Effect of *CSR* on the development of excess pore water pressures: (a) plotted against the number of cycles; (b) plotted against time

Fig. 12. Effect of PSR on the development of excess pore water pressures: (a) *CSR* = 0.2; (b) *CSR* = 0.3

Fig. 13. Degradation of resilient modulus: (a) effect of frequency for *CSR* = 0.2 (up to 50000 cycles); (b) effect of *CSR*

Fig. 14. Effect of PSR on the degradation of the resilient modulus: (a) *CSR* = 0.2; (b) *CSR* = 0.3

Fig. 15. Effect of frequency and *CSR* on the initial resilient modulus

Table 1. Properties of the kaolin, sand and reconstituted soil specimens

Soil type	Specific gravity	Liquid Limit w_L (%)	Plastic Limit w_P (%)	Plasticity Index (I_P)	USCS soil classification
Kaolin	2.7	55	27	28	Clay of high plasticity (CH)
Sand	2.61		Non-plastic		Well-graded sand (SW)
Reconstituted soil	2.66	27.5	16.7	10.8	Clay of low plasticity (CL)

Note: USCS = Unified Soil Classification System.

Table 2. Testing programme

Test Number	Cyclic Stress Ratio	Frequency (Hz)	Apparatus
T1	0.2	0.1	DYNHCA
T2	0.2	0.1	CTA
T3	0.2	0.5	DYNHCA
T4	0.2	1.0	DYNHCA
T5	0.2	1.0	CTA
T6	0.3	0.1	DYNHCA
T7	0.3	0.1	CTA
T8	0.3	0.5	DYNHCA
T9	0.3	1.0	DYNHCA
T10	0.3	1.0	CTA

Note: DYNHCA = dynamic hollow cylinder apparatus; CTA = cyclic triaxial apparatus.

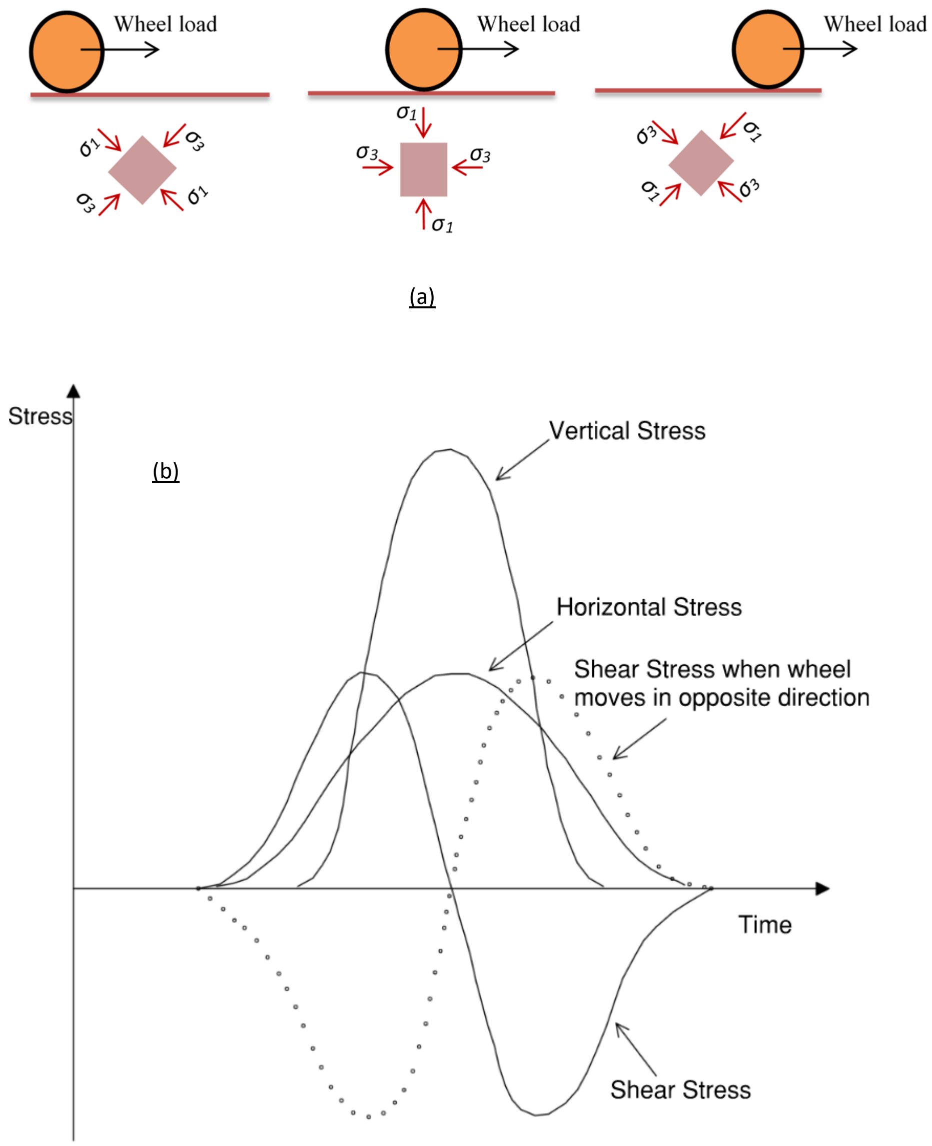

Fig. 1. (a) Principal stress rotation in soil under moving wheel loads; (b) stress conditions under a single moving wheel load (after Brown 1996)

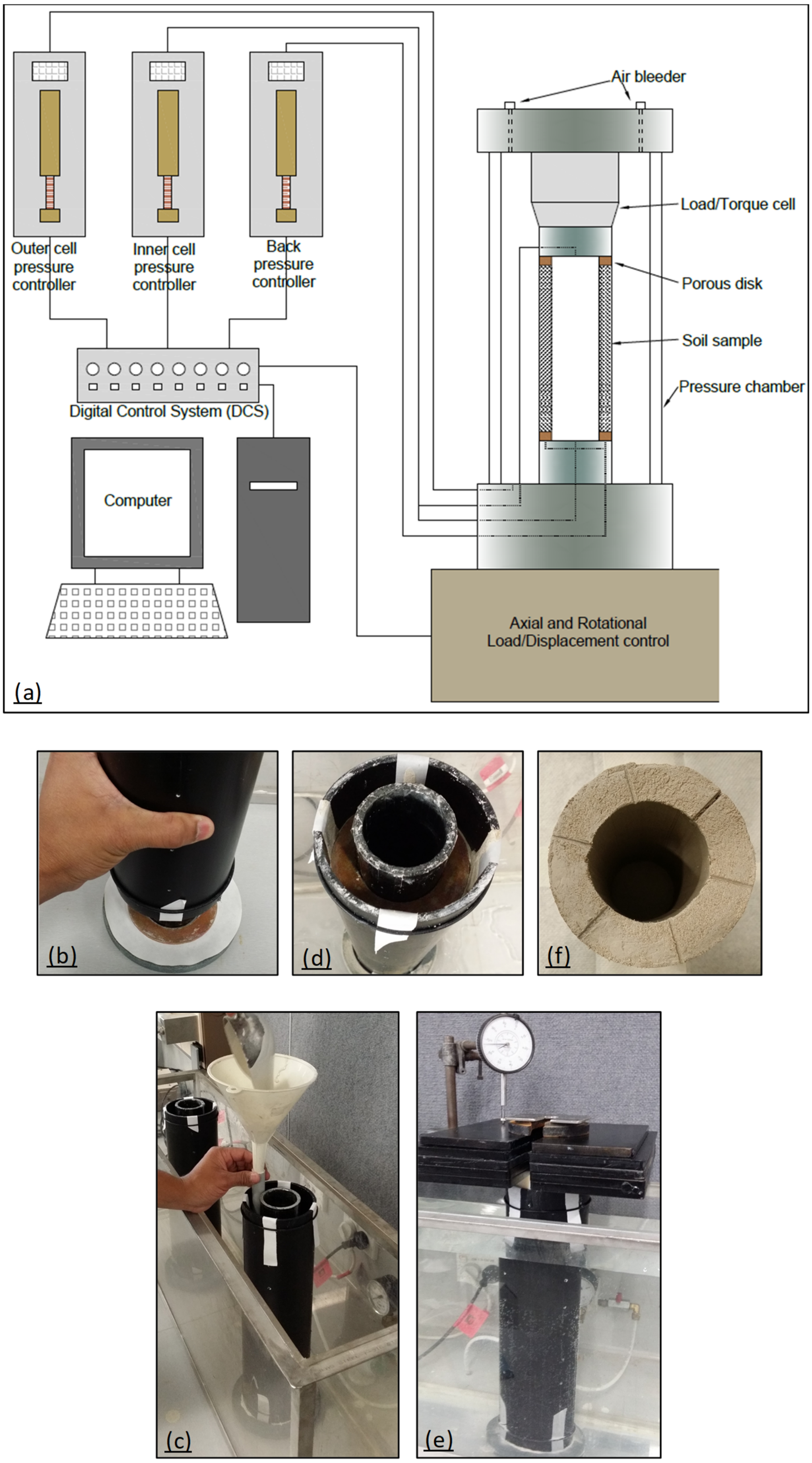

Fig. 2. (a) Schematic diagram of the hollow cylinder apparatus; (b) moulds positioned by the bottom porous disk; (c) pouring slurry; (d) top porous disk positioned over slurry; (e) consolidation; (f) grooved soil specimen

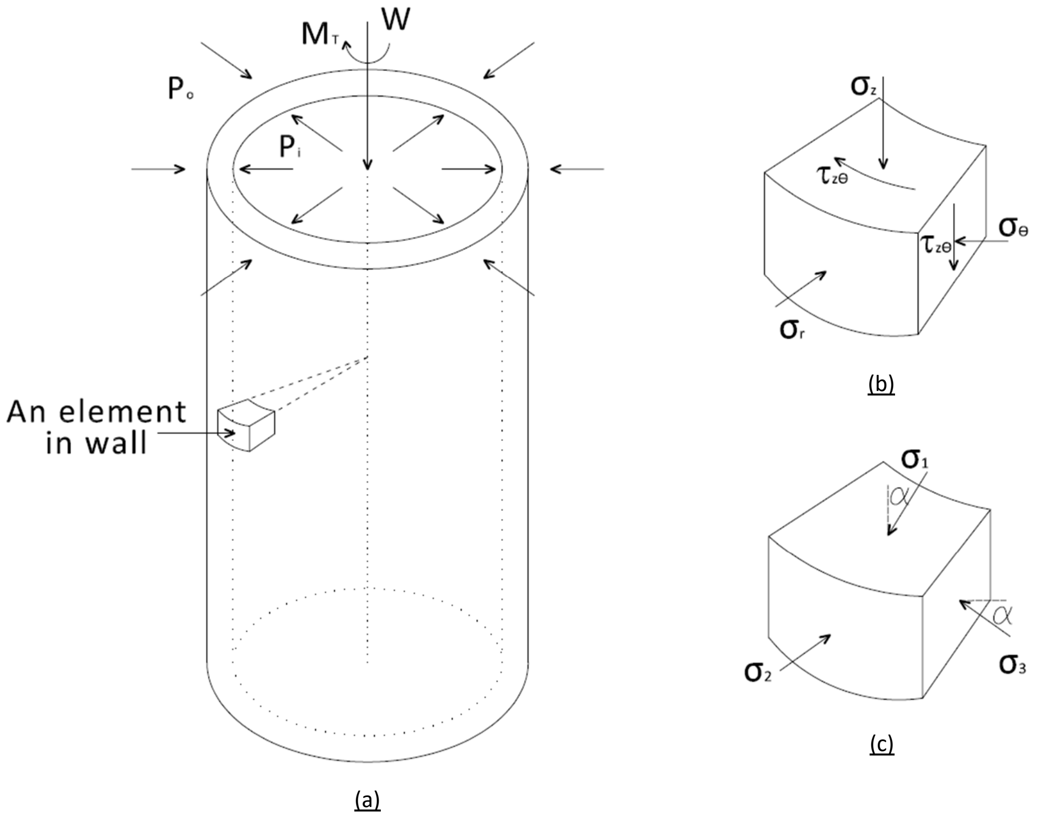

Fig. 3. Stress status in a hollow cylinder specimen: (a) external loadings; (b) local stresses on an element; (c) principal stresses on an element

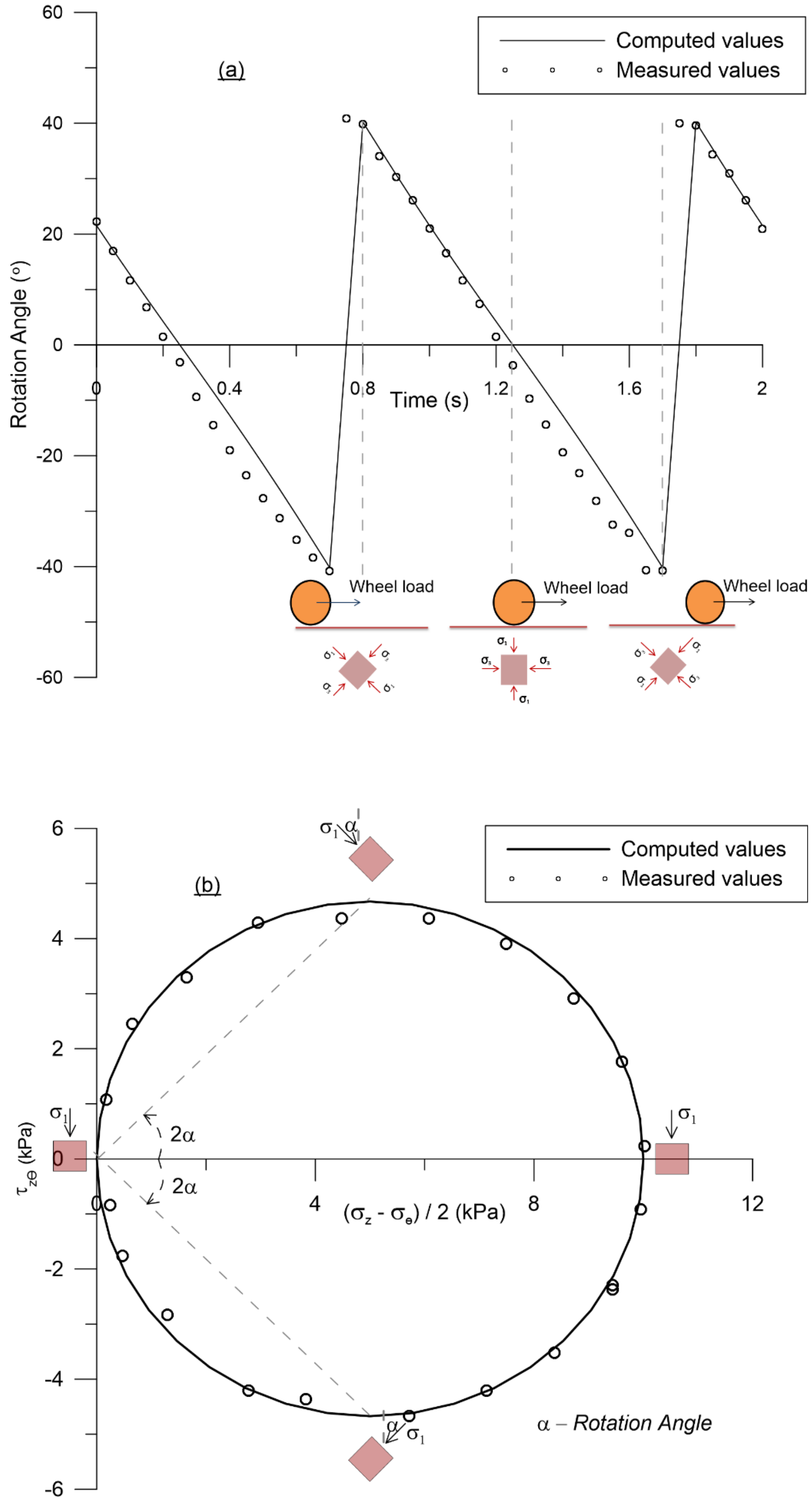

Fig. 4. Effect of moving wheel loads on: (a) rotation angle; (b) shear stresses

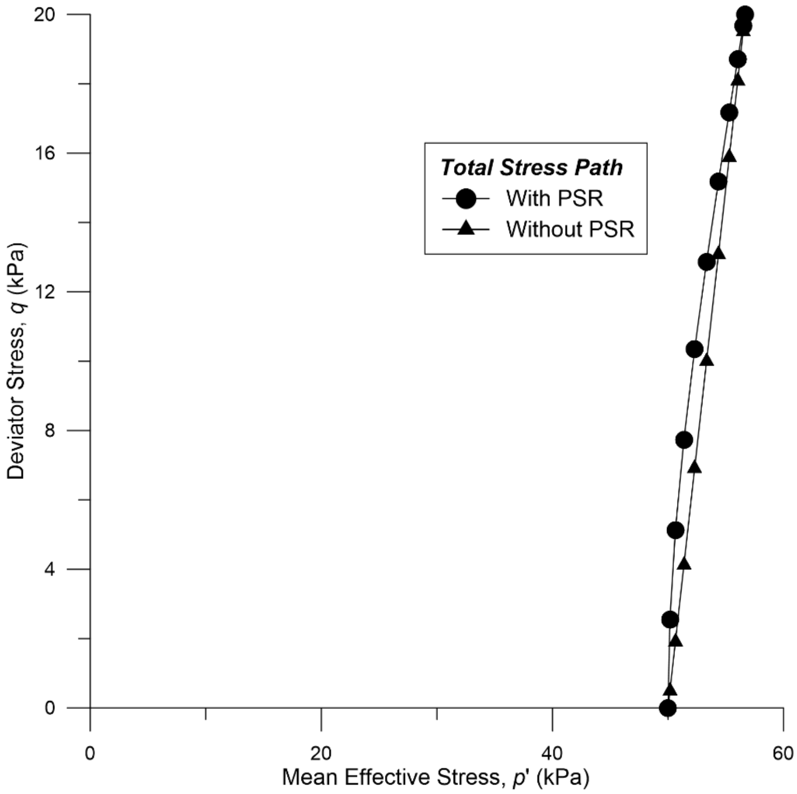

Fig. 5. Comparison of total stress path for cyclic loading with and without PSR

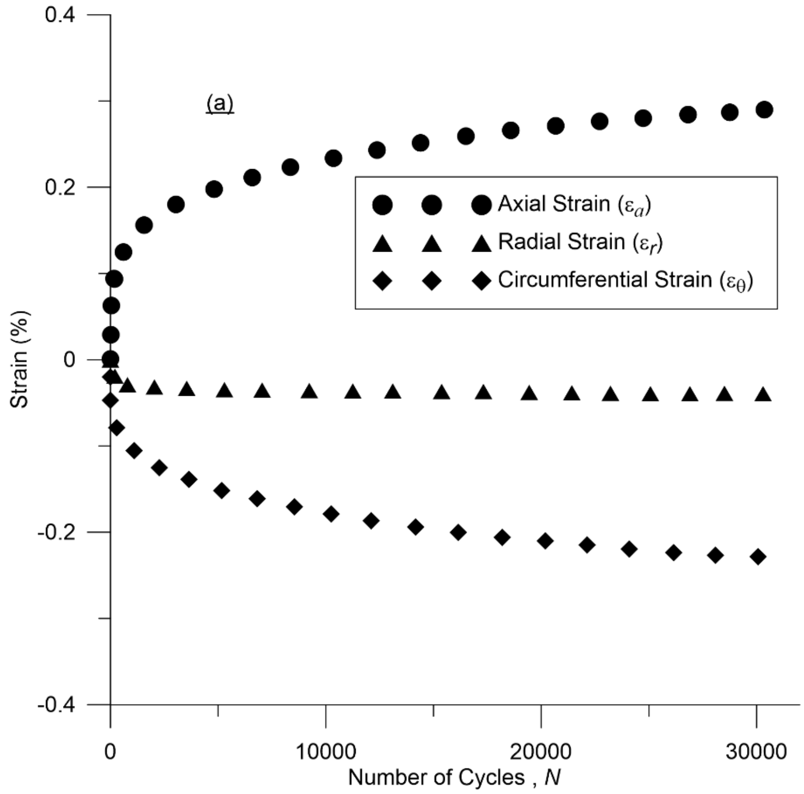

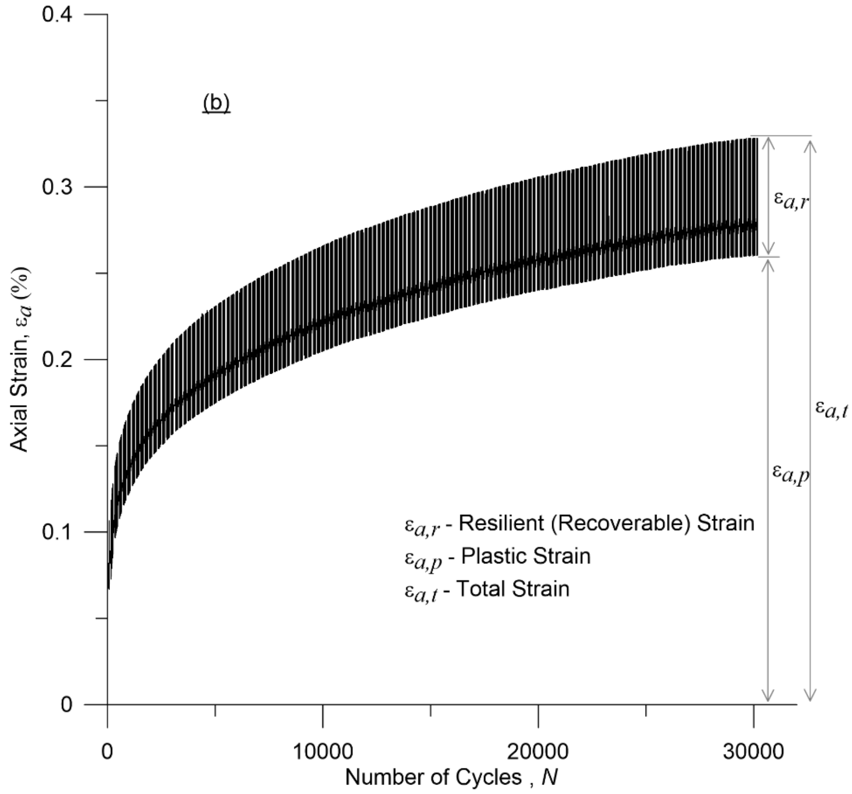

Fig. 6. (a) Variation of mean values of axial, radial and circumferential strain with the number of cycles (test T4); (b) variation of axial strain with the number of cycles showing the different strain components (test T4)

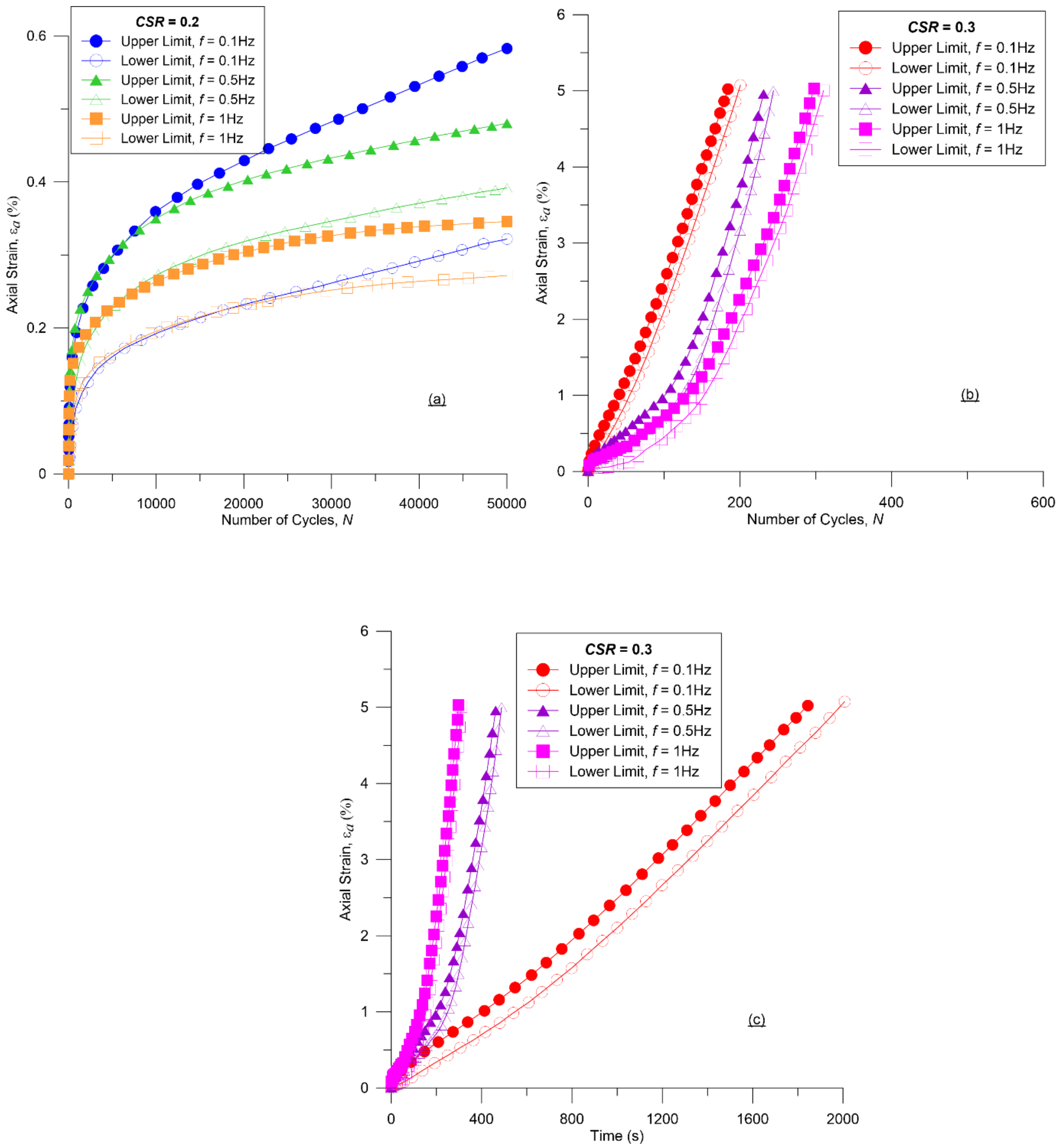

Fig. 7. Effect of frequency on the accumulation of axial deformations: (a) *CSR* = 0.2; (b) *CSR* = 0.3 (strains plotted against the number of cycles); (c) *CSR* = 0.3 (strains plotted against time)

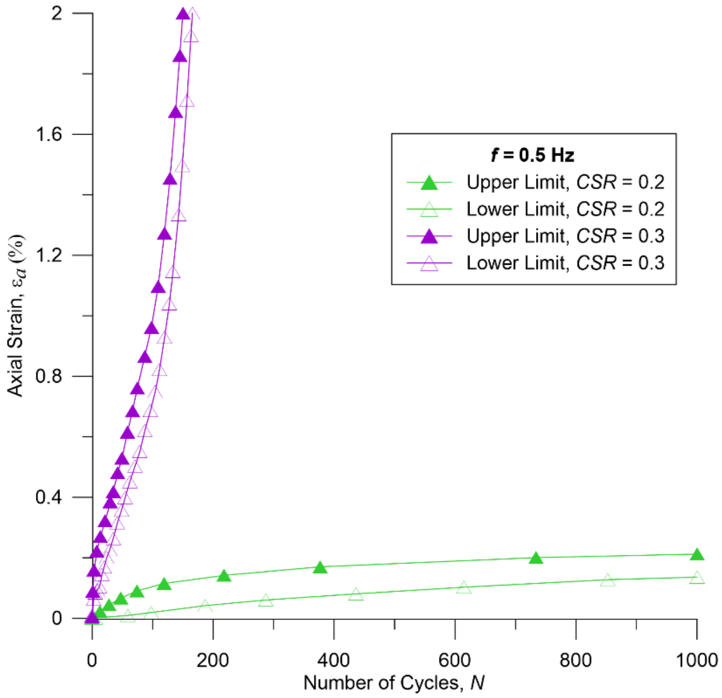

Fig. 8. Effect of *CSR* on the accumulation of axial deformations (*f* = 0.5 Hz)

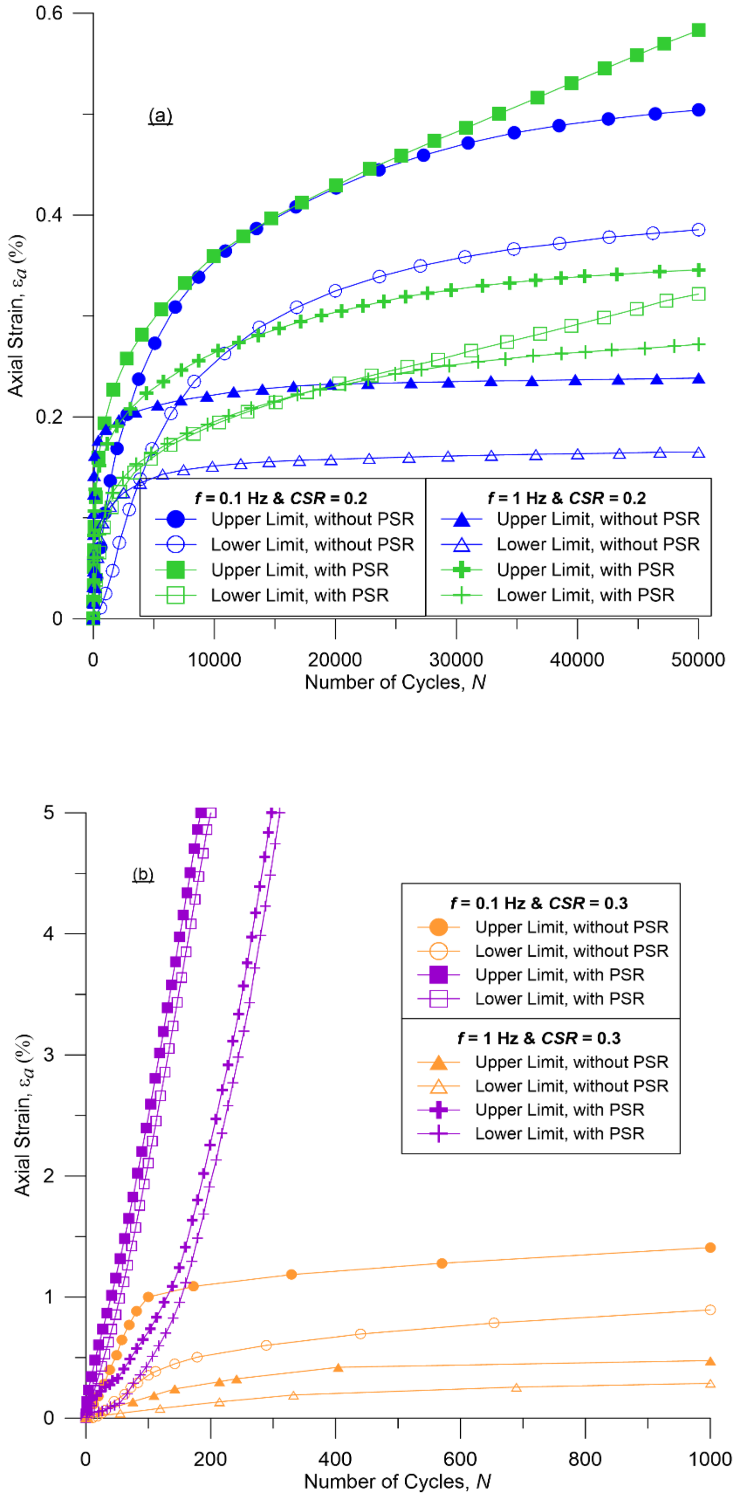

Fig. 9. Effect of PSR on the accumulation of axial deformations: (a) *CSR* = 0.2; (b) *CSR* = 0.3

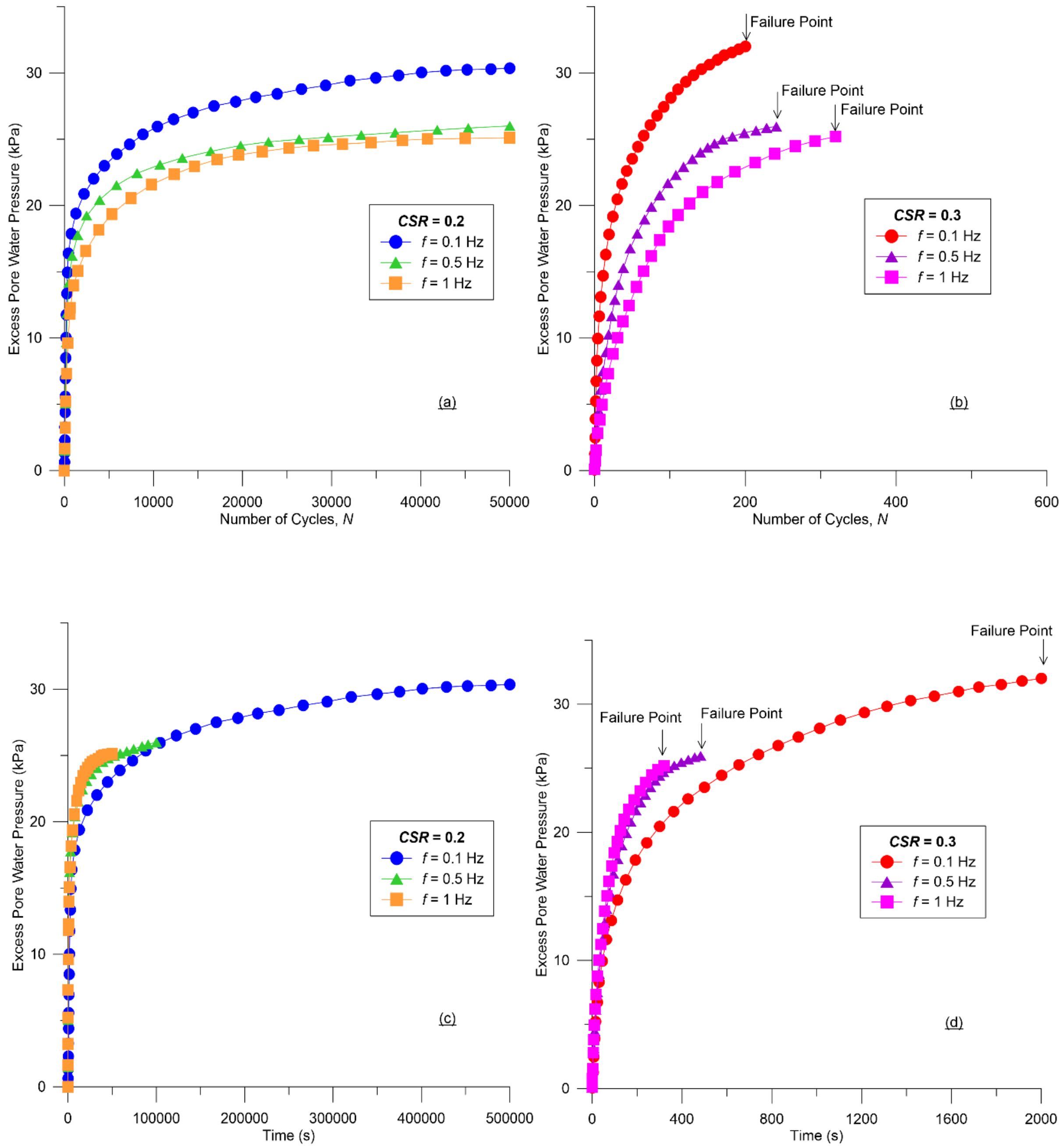

Fig. 10. Effect of frequency on the development of excess pore water pressures: (a) *CSR* = 0.2 (plotted against the number of cycles; (b) *CSR* = 0.3 (plotted against the number of cycles); (c) *CSR* = 0.2 (plotted against time); (d) *CSR* = 0.3 (plotted against time)

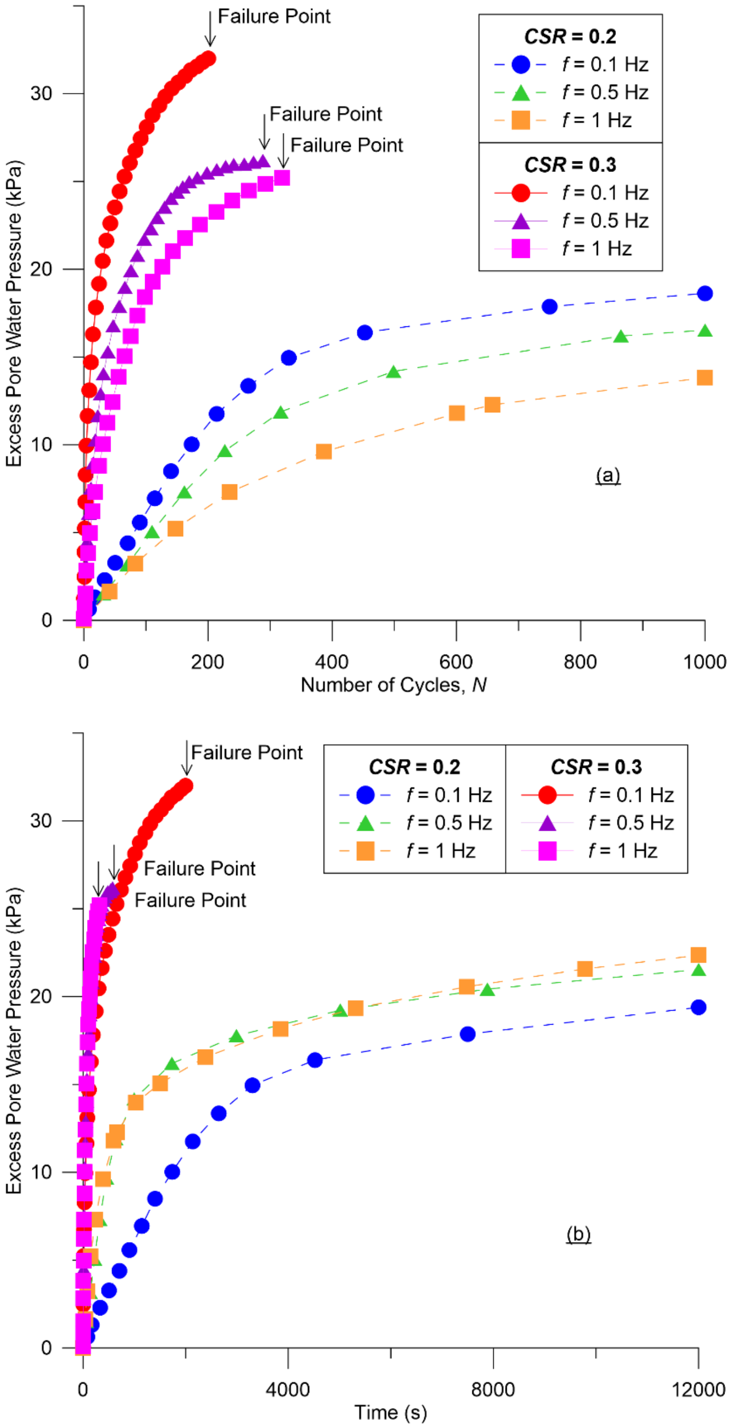

Fig. 11. Effect of *CSR* on the development of excess pore water pressures: (a) plotted against the number of cycles; (b) plotted against time

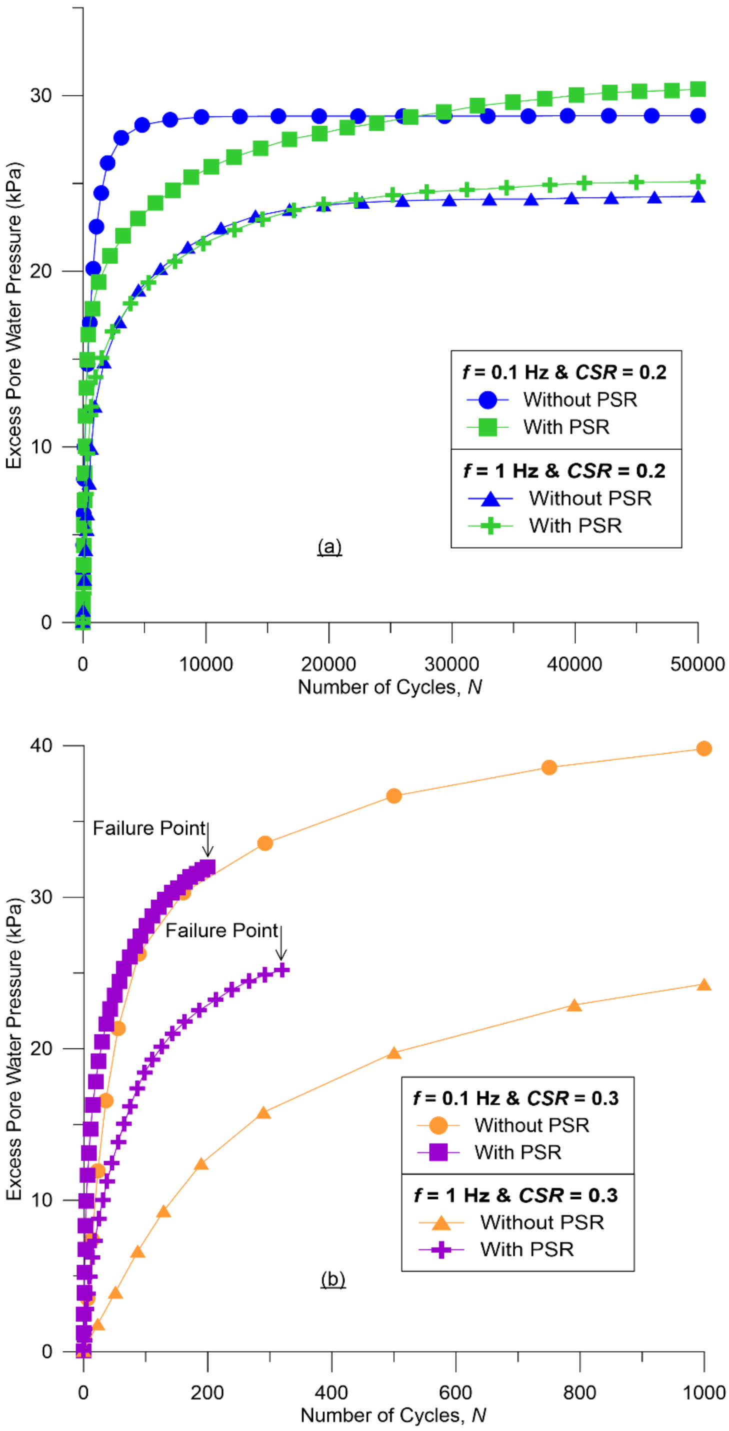

Fig. 12. Effect of PSR on the development of excess pore water pressures: (a) *CSR* = 0.2; (b) *CSR* = 0.3

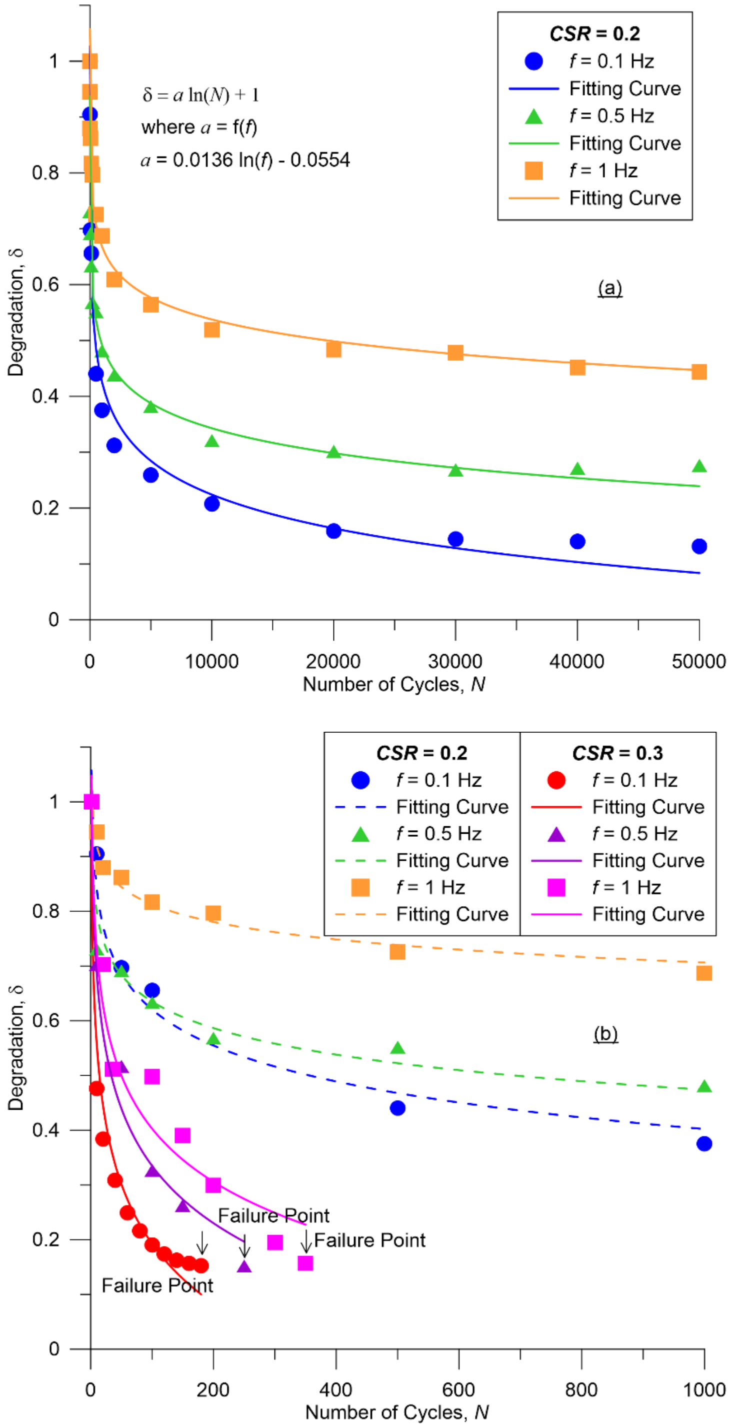

Fig. 13. Degradation of resilient modulus: (a) effect of frequency for *CSR* = 0.2 (up to 50000 cycles); (b) effect of *CSR*

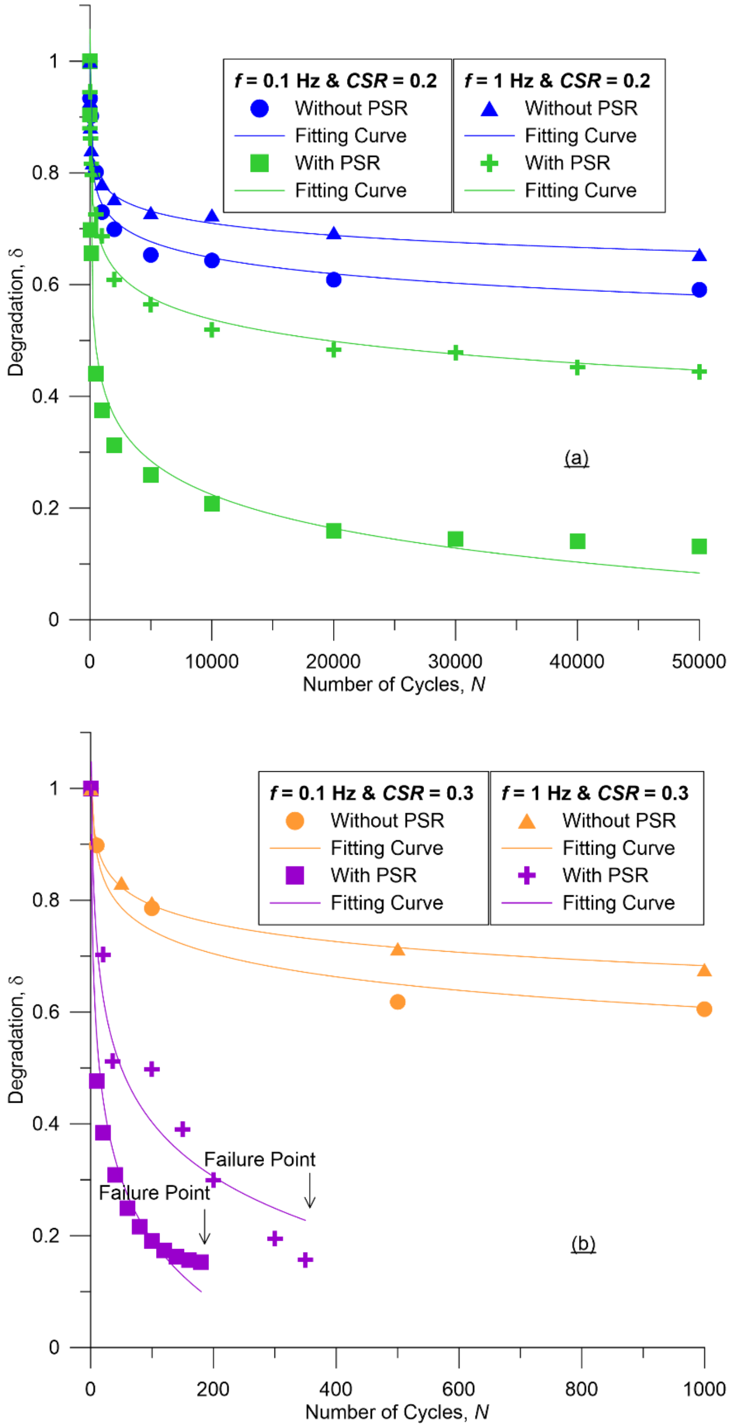

Fig. 14. Effect of PSR on the degradation of the resilient modulus: (a) *CSR* = 0.2; (b) *CSR* = 0.3

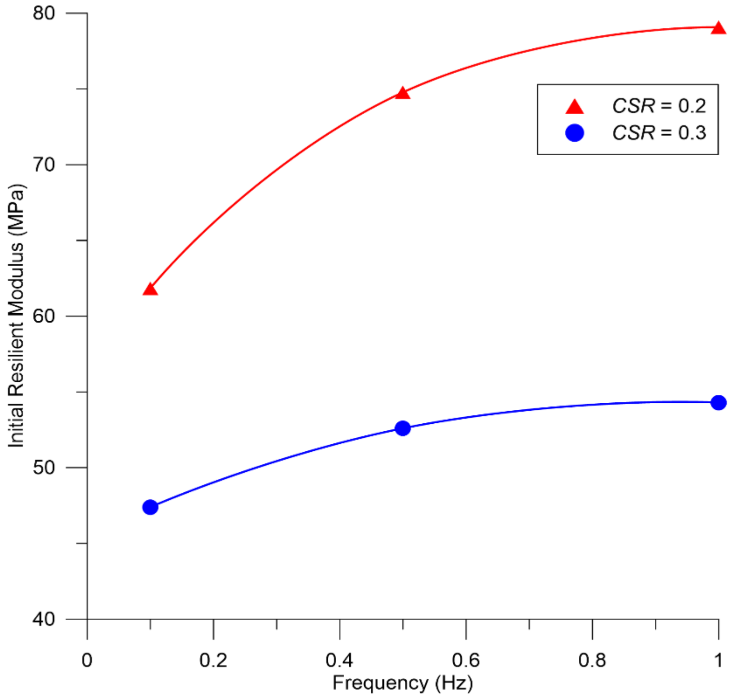

Fig. 15. Effect of frequency and *CSR* on the initial resilient modulus